

SPC 307

Introduction to Aerodynamics

Lecture 10

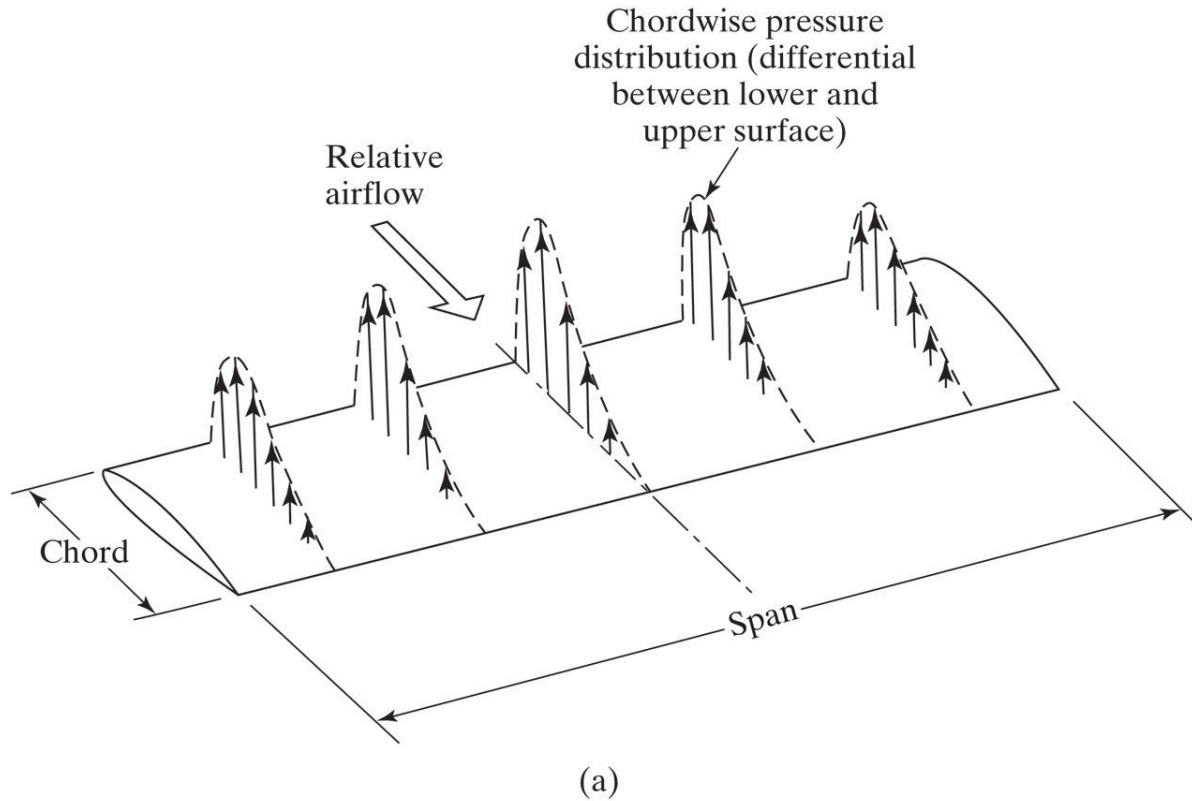
INCOMPRESSIBLE FLOWS ABOUT
WINGS OF FINITE SPAN

May 14, 2017

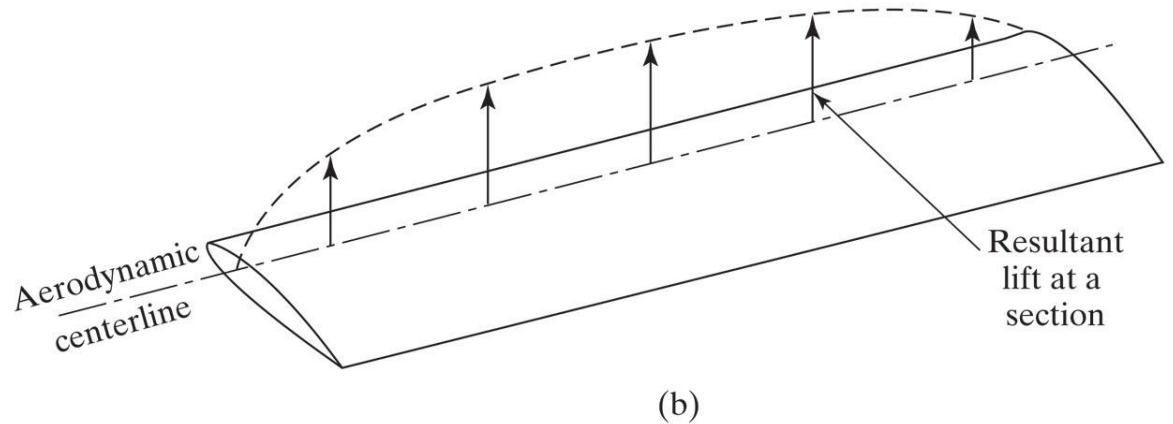
GENERAL COMMENTS

- Pressure variations can be sensed between the upper and lower surfaces of a wing.
- The low-pressure region over the wing causes fluid from the high-pressure region below the wing to flow around the wing tip, creating a vortex in the region of the wing tip.
- As a consequence, **the lift force per unit span decreases toward the wing tips.**
- In Fig. 7.1 a, there is a chordwise variation in the pressure differential between the lower surface and the upper surface.
- In Fig. 7.1 b, there is a spanwise variation in the lift force.
- As a result of the spanwise pressure variation, the air on the **upper surface flows inboard** toward the root.
- Similarly, on the **lower surface, air will tend to flow outward** toward the wing tips.

Aerodynamic load distribution for a rectangular wing in subsonic airstream:



- (a) differential pressure distribution along the chord;
- (b) lift distribution.

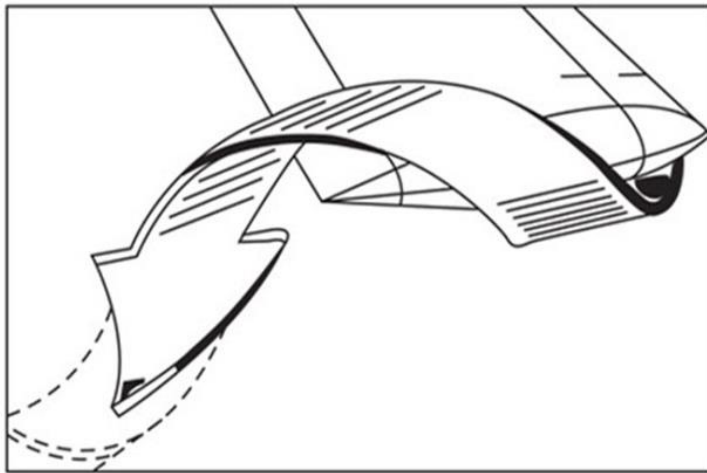
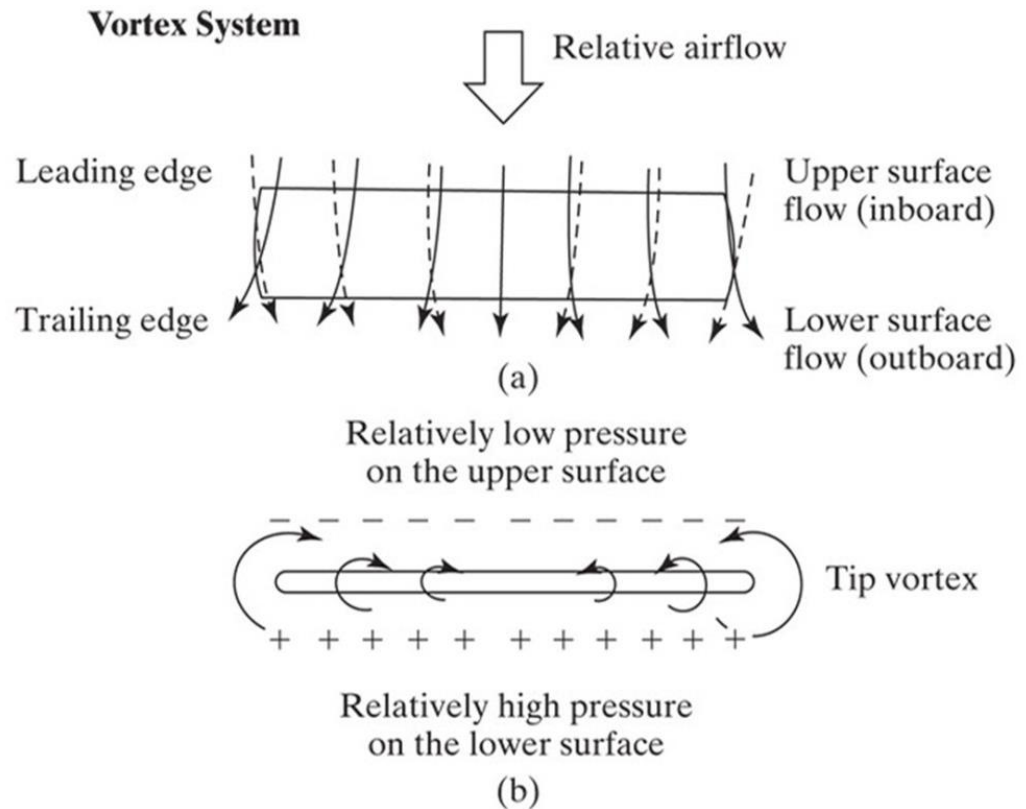


Tip Vortices

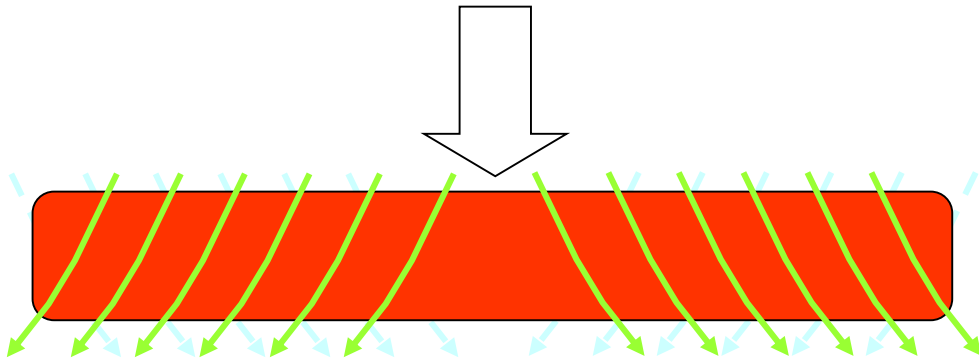
- The flows from the upper surface and the lower surface join at the trailing edge, the difference in spanwise velocity components will cause the air to roll up into a number of streamwise vortices, distributed along the span.
- These small vortices roll up into two large vortices just inboard of the wing tips (Fig. 7.2).
- Very high velocities and low pressures exist at the core of the wing-tip vortices.
- In many instances, water vapor condenses as the air is drawn into the low-pressure flow field of the tip vortices.
- Condensation clearly defines the tip vortices of the Shuttle Orbiter *Columbia* on approach to a landing at Kennedy Space Center (Fig. 7.3), where the vortices are very evident due to the high water vapor content of the air at this geographic location.

Generation of the trailing vortices due to the spanwise load distribution:

- (a) view from bottom;
- (b) view from trailing edge;
- (c) formation of the tip vortex

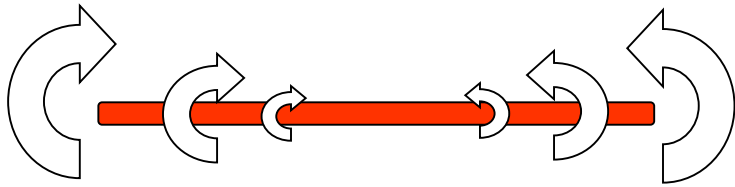


(c)

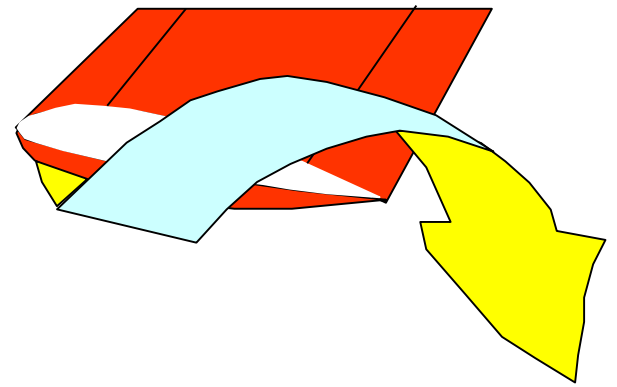


From bottom

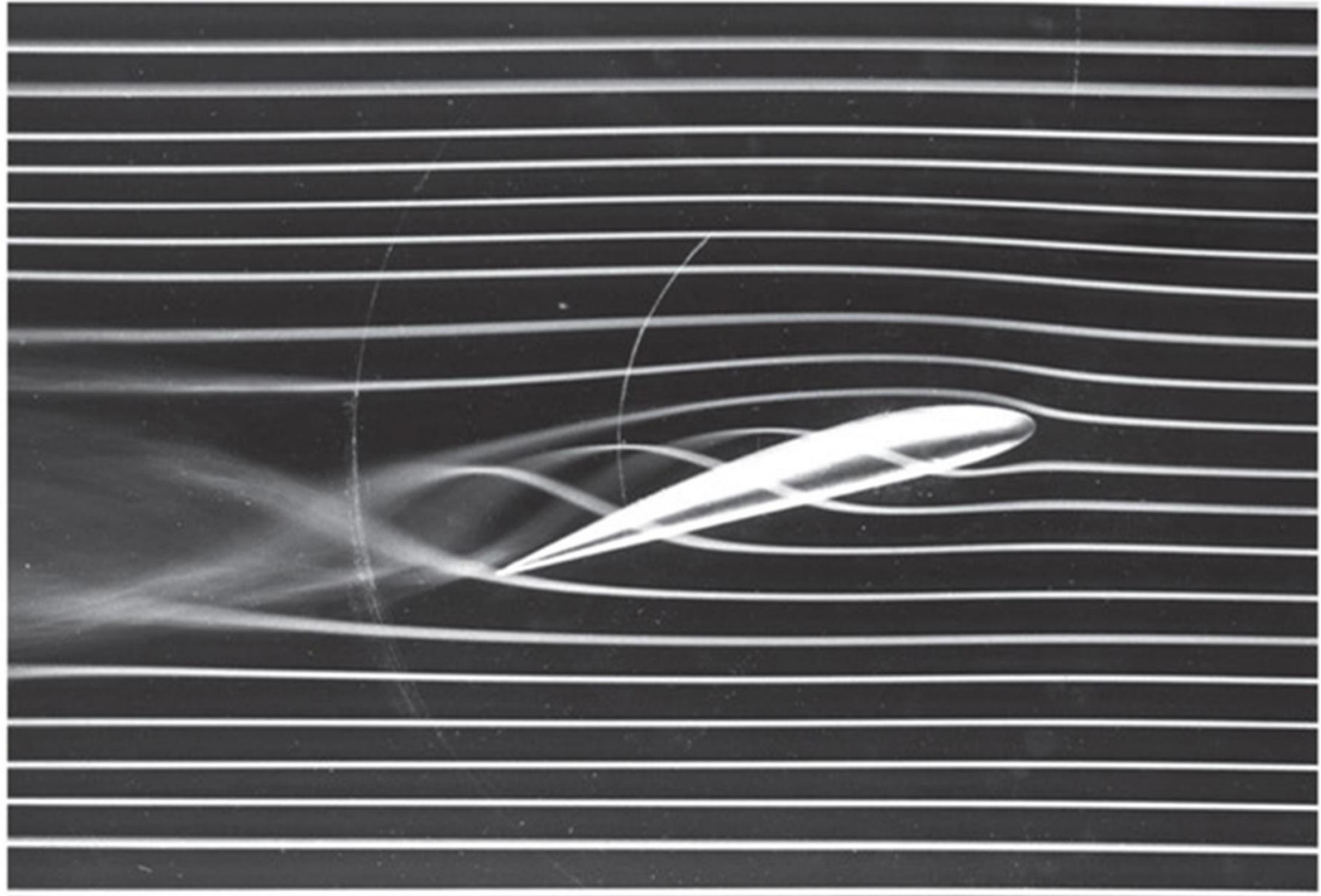
Low Pressure



High Pressure



Smoke-flow pattern showing tip vortex.



(d)

Condensation marks the wing-tip vortices of the Space Shuttle Orbiter *Columbia*.







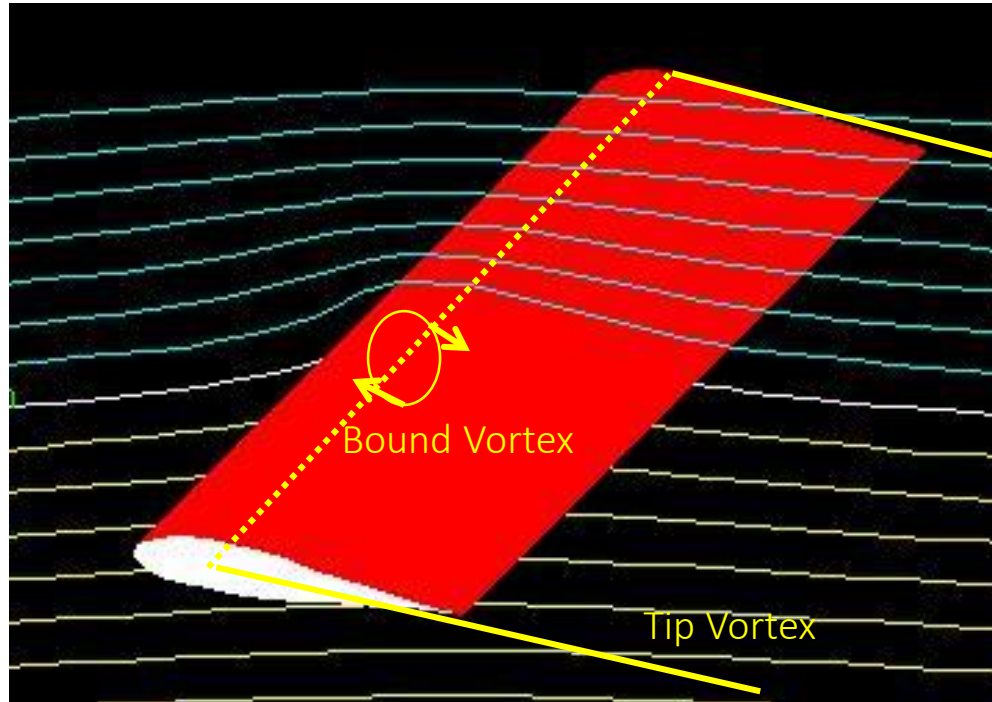
Vortex System

- In order to model the flow of air around the wing mathematically, we customarily assume:
 1. that the vortex wake, which is of finite thickness, may be replaced by an infinitesimally thin surface of discontinuity, designated the trailing vortex sheet, and
 2. that the trailing vortex sheet remains flat as it extends downstream from the wing.
- An important difference in the 3-D flow field around a wing (as compared with the 2-D flow around an airfoil) is the spanwise variation in lift.
- Since the lift force acting on the wing section at a given spanwise location is related to the strength of the circulation, there is also a corresponding spanwise variation in circulation, such that the circulation at the wing tip is zero (**the lift at the wing tip is zero?**).
- A suitable distribution of vortices would represent the physical wing in every way except that of thickness.

VORTEX SYSTEM

- In Prandtl's approach, the vortex system consists of:
 - the bound vortex system
 - the trailing vortex system
 - the "starting" vortex
- The "starting" vortex is associated with a change in circulation that might occur as the wing begins moving or as the angle of attack changes during flight.
- The representation of the wing by a bound vortex allows a relation to be established between:
 - the physical load distribution for the wing (which depends on the wing geometry and on the aerodynamic characteristics of the wing sections) and the trailing vortex system
- This relation allows to quantify the impact of the trailing vortex system on the lift and drag of the wing, and the difference between the wing airfoil sections and the infinite-span airfoil sections.

Prandtl Lifting Line Theory (PLLT)



Three dimensional version of Bound Vortex Theory

A continuous line of bound vortices terminating at the wing tips with “tip vortices” that continue downstream to the “starting vortex”.

LIFTING-LINE THEORY FOR UNSWEPT WINGS

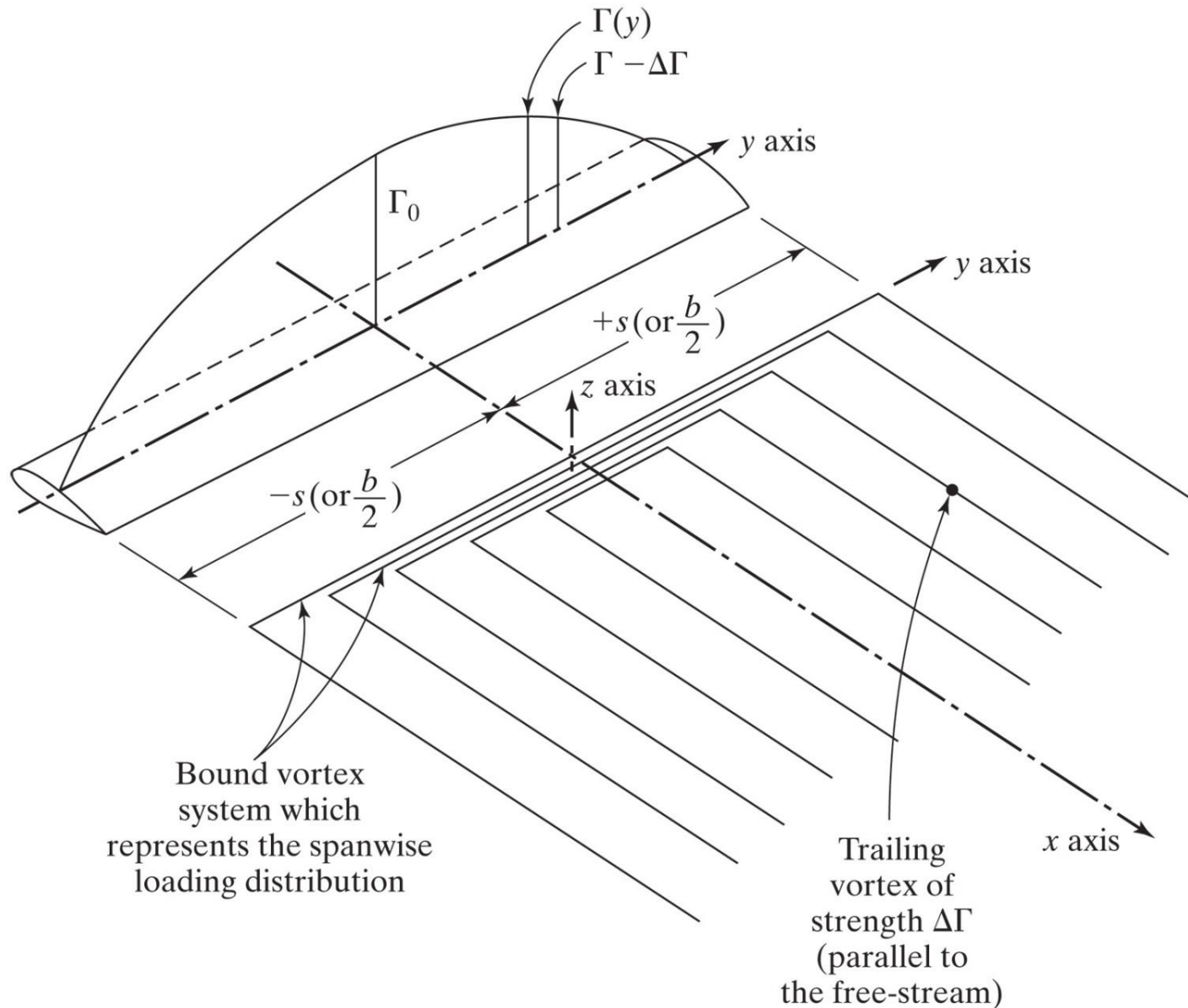
- We are interested in developing a model that can be used to estimate the aerodynamic characteristics of a wing which is unswept (or is only slightly swept) and which has an aspect ratio of 4.0 or greater.
- The spanwise variation in lift, $l(y)$, is similar to that in Fig. 7.1 b.
- Prandtl and Tietjens (1957) hypothesized that *each airfoil section of the wing acts as an isolated two-dimensional section, provided that the spanwise flow is not too great.*
- Each section of the finite-span wing generates a section lift equivalent to that acting on a similar section of an infinite-span wing having the same section circulation.
- The lift acting on an incremental span-wise element of the wing is related to the local circulation through the Kutta-Joukowski theorem. That is,

$$l(y) = \rho_{\infty} U_{\infty} \Gamma(y)$$

LIFTING-LINE THEORY FOR UNSWEPT WINGS

- In Prandtl's approach, the spanwise lift distribution is represented by a system of vortex filaments, the axis of which is normal to the plane of symmetry and which passes through the aerodynamic center of the lifting surface.
- The aerodynamic center is at the quarter chord, we will place the bound-vortex system at the quarter-chord line.
- The strength of the bound-vortex system at any location (y) is proportional to the local lift acting at that location $\ell (y)$.
- **Helmholtz** stated that a vortex filament has constant strength along its length. Therefore, we will model the lifting character of the wing by a large number of vortex filaments (i.e., a large bundle of infinitesimal-strength filaments) that lie along the quarter chord of the wing.
- This is the bound-vortex system, which represents the spanwise loading distribution, as shown in Fig. 7.4 (a), and is known as the *lifting line* .

7.4.a. Schematic trailing-vortex system.



- At any location y , the sum of the strengths of all of the vortex filaments in the bundle at that station is $\Gamma(y)$.
- When the lift changes at some location, the total strength of the bound-vortex system changes proportionally [i.e., $\Delta\Gamma(y)$].
- But **Helmholtz** also stated that vortex filaments cannot end in the fluid. Therefore, the change $\Delta\Gamma(y)$ is represented by having some of the filaments from our bundle of filaments turn 90° and continue in the streamwise direction (i.e., in the x direction).
- The strength of the trailing vortex at any y location is equal to the change in the strength of the bound-vortex system.
- The strength of the vortex filaments continuing in the bound-vortex system depends on the spanwise variation in lift and, therefore, depends upon geometric parameters such as the wing planform, the airfoil sections that make up the wing, the geometric twist of the wing, etc.
- If the strength of the vortex filaments in the bundle changes by the amount $\Delta\Gamma$, a trailing vortex of strength $\Delta\Gamma$ must be shed in the x direction.

LIFTING-LINE THEORY FOR UNSWEPT WINGS

- The vortex filaments that make up the bound-vortex system do not end in the fluid when the lift changes, but turn backward at each end to form a pair of vortices in the trailing-vortex system.
- For steady flight conditions, *the starting vortex is left far behind, so that the trailing-vortex pair effectively stretches to infinity.*
- The three-sided vortex, which is termed a *horseshoe vortex*, is presented in Fig. 7.4 a.
- For practical purposes, the system consists of the bound-vortex system and the related system of trailing vortices.
- Also included in Fig. 7.4 a is a sketch of a symmetrical lift distribution (the variation is the same on each half of the wing), which the vortex system represents.

Vortex System

- A number of vortices are made visible by using a smoke generation system for the flow over a **Boeing 747 wing**. Flow from the wing tip region and two other locations can be seen leaving the trailing edge on each wing and then rolling up into two counter-rotating vortices.
- This shows why it is important to include shed vorticity from along the entire span.
- These streamwise vorticity filaments correspond to the trailing vortices shed by the spanwise variation in vorticity across the wing.
- Conventional Prandtl lifting-line theory (PLLT) provides reasonable estimates of the lift and induced drag until boundary-layer effects become important.
- Therefore, there will be reasonable agreement between the calculations and the experimental values for a single lifting surface having no sweep, no dihedral, and an aspect ratio of 4.0 or greater, operating at relatively low angles of attack.

Streamwise vorticity shedding along the trailing edge of a Boeing 747 rolling up into wing-tip vortices.







A



- An aircraft of a lower wake vortex category must not be allowed to take off less than two minutes behind an aircraft of a higher wake vortex category
- American Airlines Flight 587 crashed into the Belle Harbor neighborhood of Queens in New York City shortly after takeoff from John F. Kennedy International Airport on November 12, 2001. This was the second deadliest U.S. aviation accident to date.

Table 2: IFR Minimum Separation Rules on Approach (nm)

Leading aircraft type ^a	Trailing aircraft type ^a		
	Small	Large	Heavy
Small	3.0	3.0	3.0
Large	4.0	3.0	3.0
Heavy	6.0	5.0	4.0

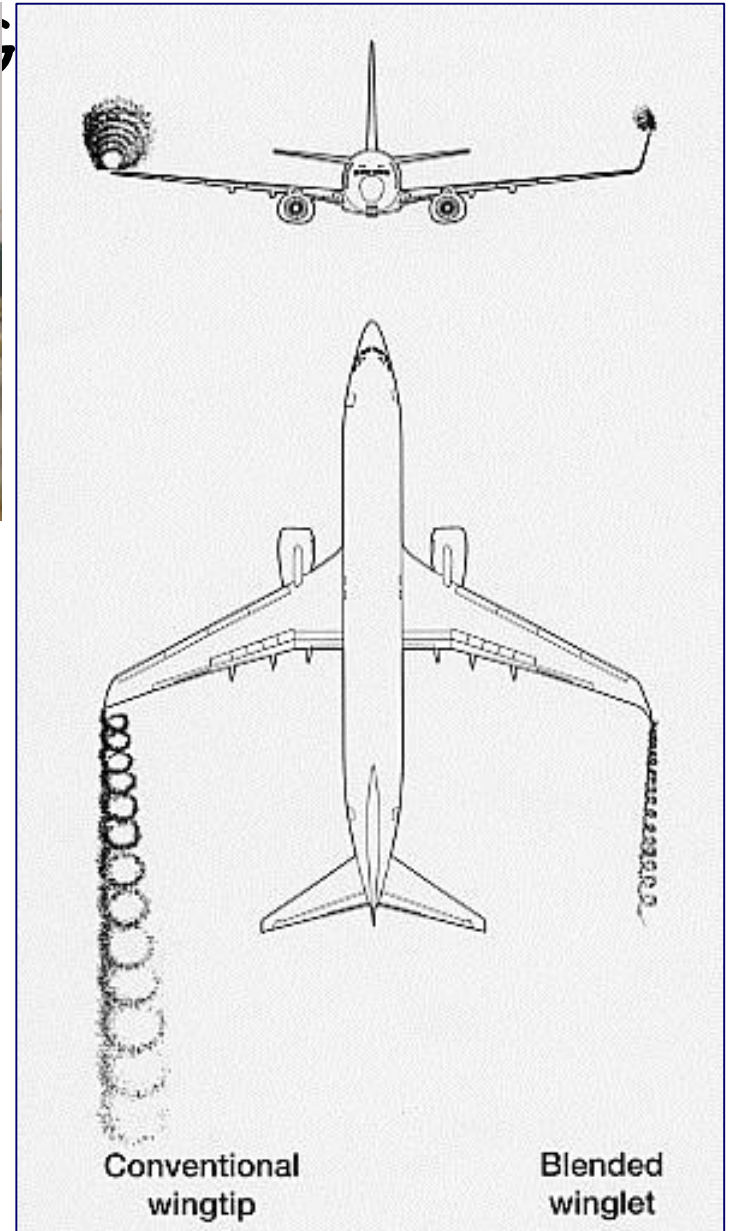
Source: FAA [1978]

* Small: aircraft weighting no more than 12,500 lb. (5,625 kg)

Large: aircraft weighting more than 12,500 lb. (5,625 kg) and less than 300,000 lb. (135,000 kg)

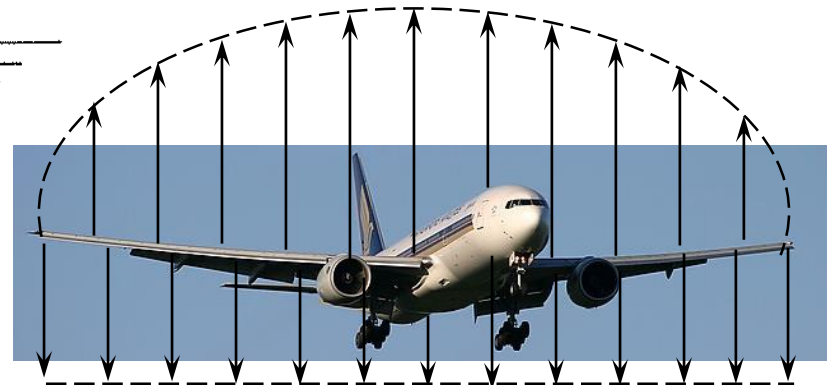
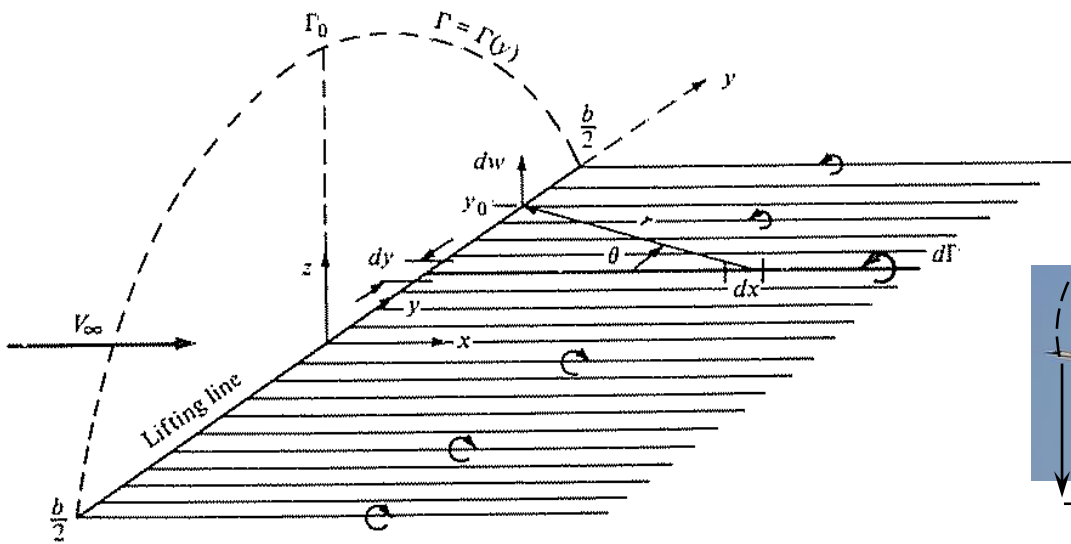
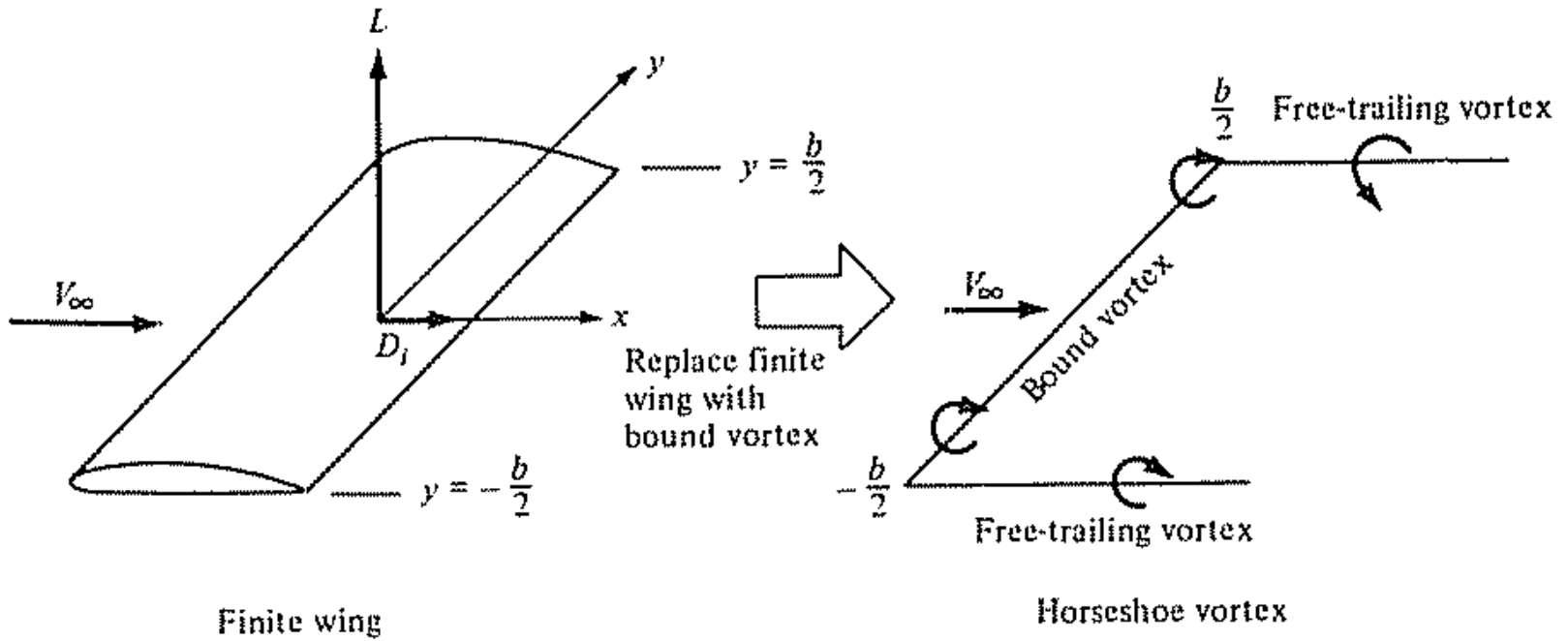
Heavy: aircraft weighting in excess of 300,000 lb. (135,000 kg)

A **nautical mile (nm)** is a unit of distance, set by international agreement as 1852 meters.

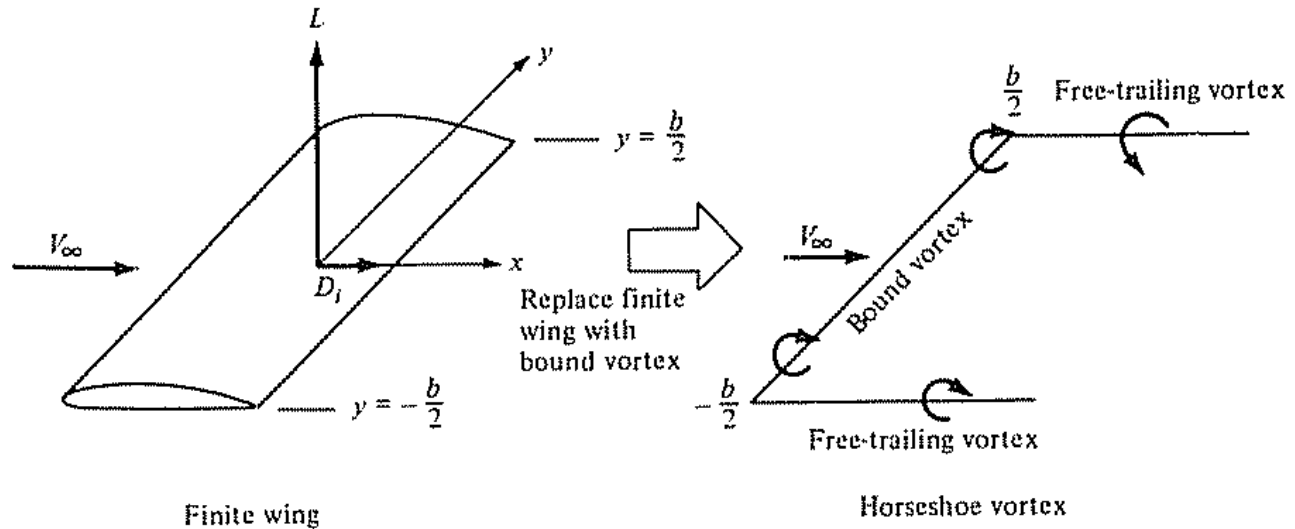


Conventional wingtip

Blended winglet



Note: Horseshoe Vortex



- Replace finite wing (span = b) with bound vortex filament extending from $y = -s = -b/2$ to $y = s = b/2$ and origin located at center of bound vortex (center of wing)
- Helmholtz's vorticity theorem: A vortex filament cannot end in a fluid
 - Filament continues as two free vortices trailing from wing tips to infinity
 - This is called a '**Horseshoe Vortex**'

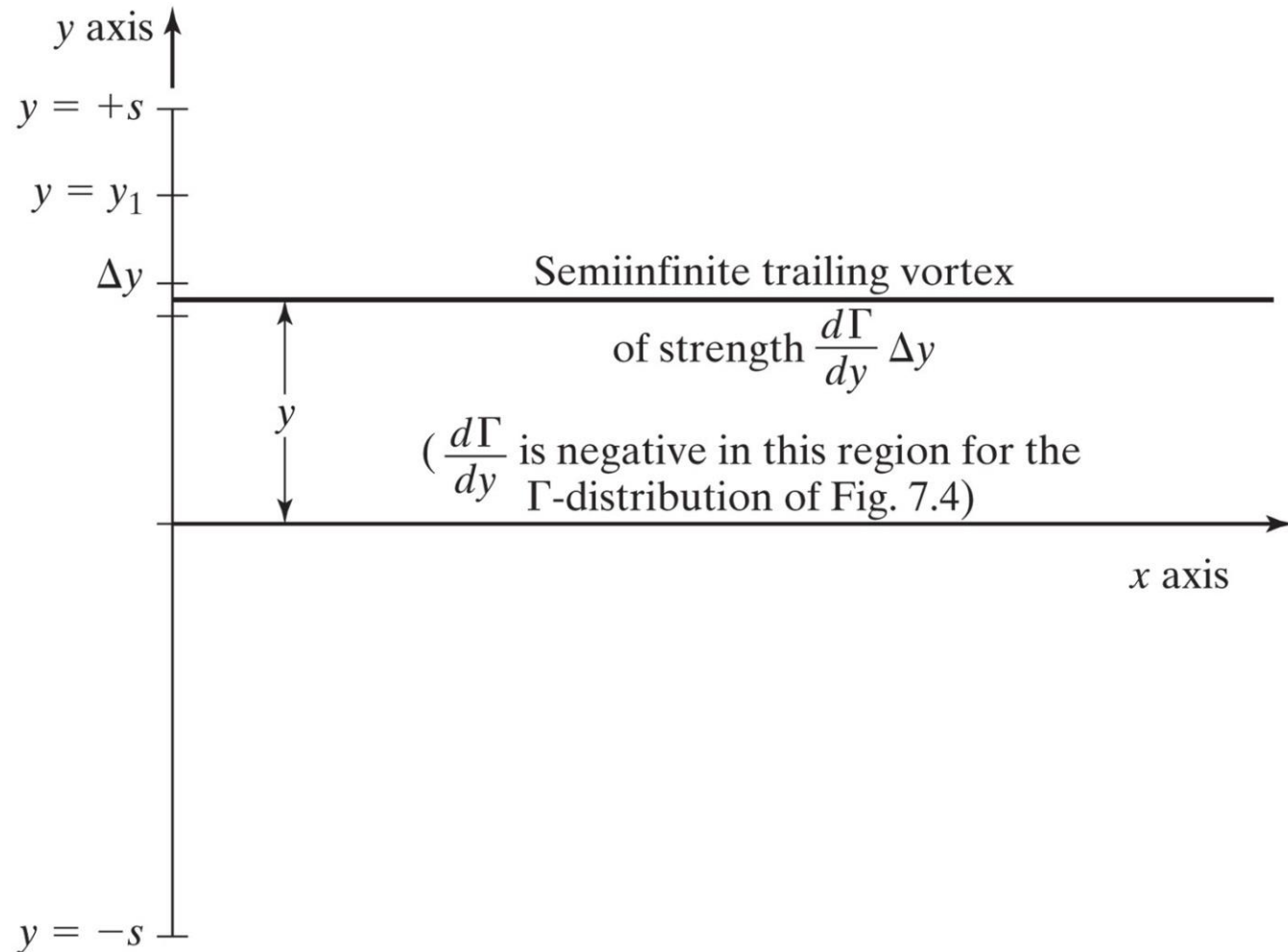
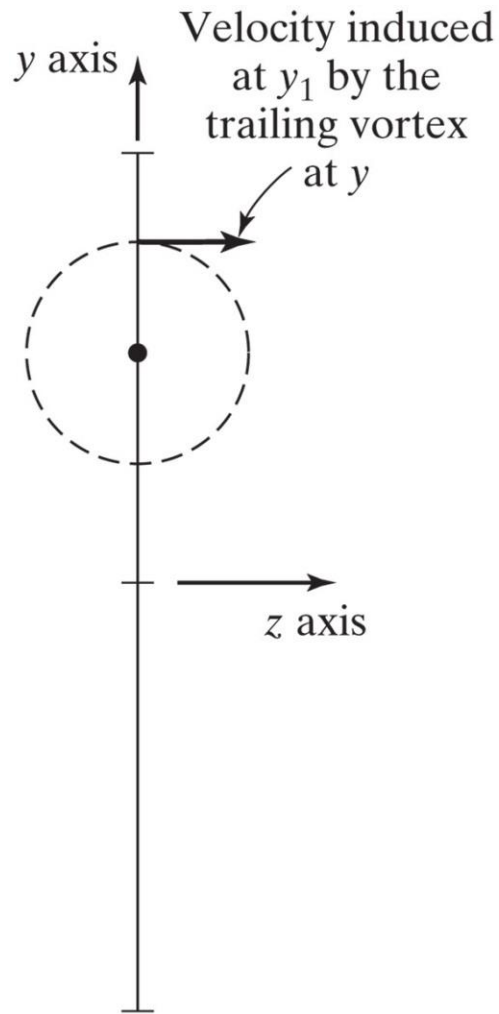
Trailing Vortices and Downwash

- A consequence of the vortex theorems of *Helmholtz* is that a bound-vortex system does not change strength between two sections unless a vortex filament equal in strength to the change joins or leaves the vortex bundle.
- If $\Gamma(y)$ denotes the strength of the circulation along the y axis a semi-infinite vortex of strength $\Delta\Gamma$ trails from the segment y .
- The strength of the trailing vortex is given by:

$$\Delta\Gamma = \frac{d\Gamma}{dy} \Delta y$$

- Assume that each spanwise strip of the wing (Δy) behaves as if the flow were locally 2-D.
- Consider the semi-infinite vortex line, parallel to the x axis (parallel to the free-stream flow) and extending downstream to infinity from the line through the aerodynamic center of the wing.
- The vortex at y induces a velocity at a general point y_1 on the aerodynamic centerline, δw_{y_1} :

Geometry for the calculation of the induced velocity at $y = y_1$.



Trailing Vortices and Downwash

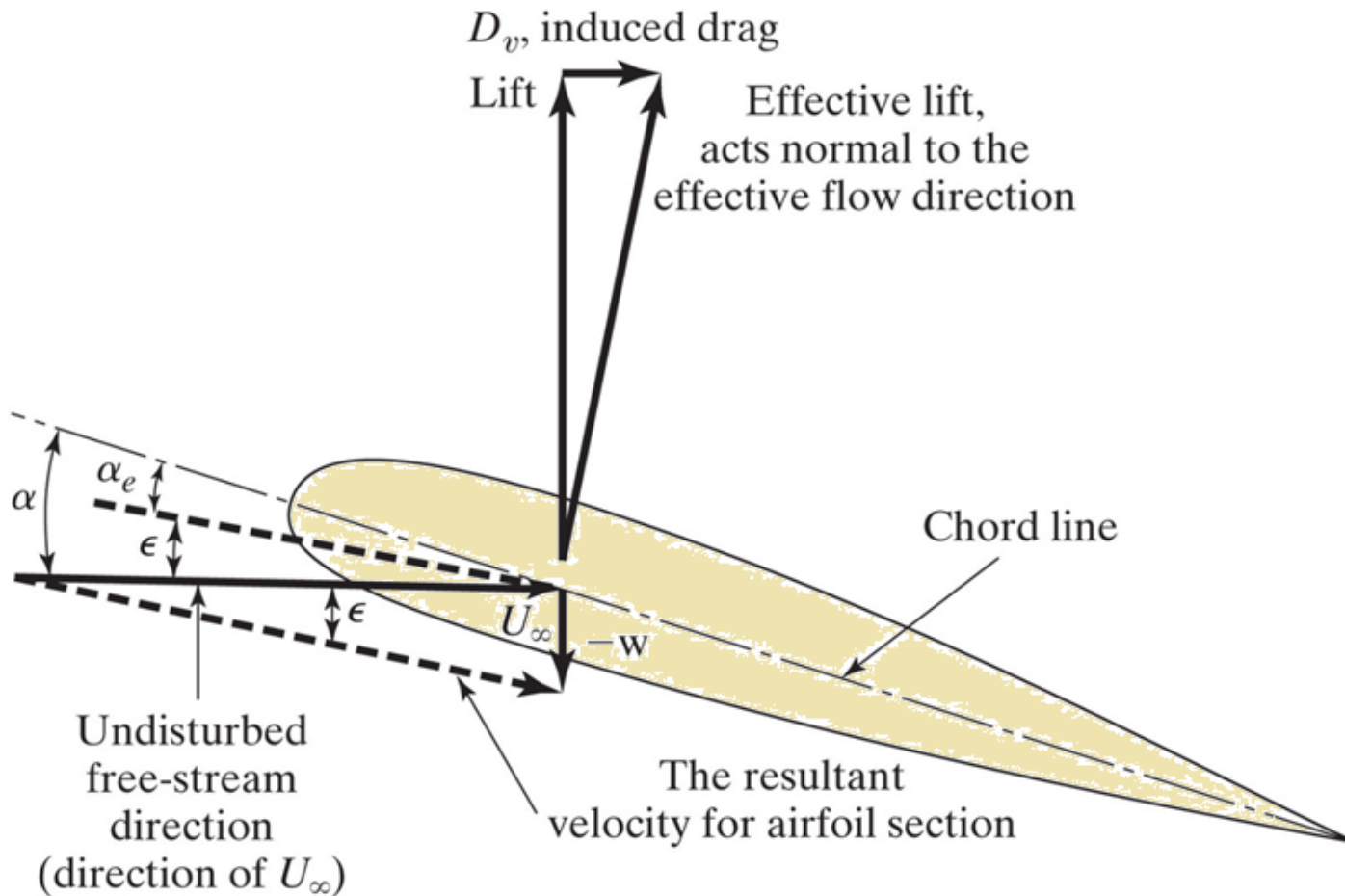
$$\delta w_{y_1} = \frac{1}{2} \left[\frac{d\Gamma}{dy} dy \frac{1}{2\pi(y - y_1)} \right]$$

- To calculate the resultant induced velocity at any point y_1 due to the cumulative effect of all the trailing vortices, the preceding expression is integrated with respect to y from the left wing tip ($-s$) to the right wing tip ($+s$) ($s = b/2$):

$$w(y_1) = -\frac{1}{4\pi} \int_{-s}^s \frac{\left(\frac{d\Gamma}{dy} \right)}{(y - y_1)} dy$$

- The resultant induced velocity at y_1 is w in a downward direction (i.e., negative, since the majority of filaments are rotating in that direction) and is called *the downwash*.
- As shown in the sketch of Fig. 7.6, the downwash angle is ε

7.6- Induced flow.



- — — Chord line of the airfoil
- - - - Effective flow direction
- Undisturbed free-stream direction

Downwash

$$\varepsilon(y_1) = \tan^{-1}\left(\frac{-w(y_1)}{U_\infty}\right) \cong \frac{-w(y_1)}{U_\infty}$$

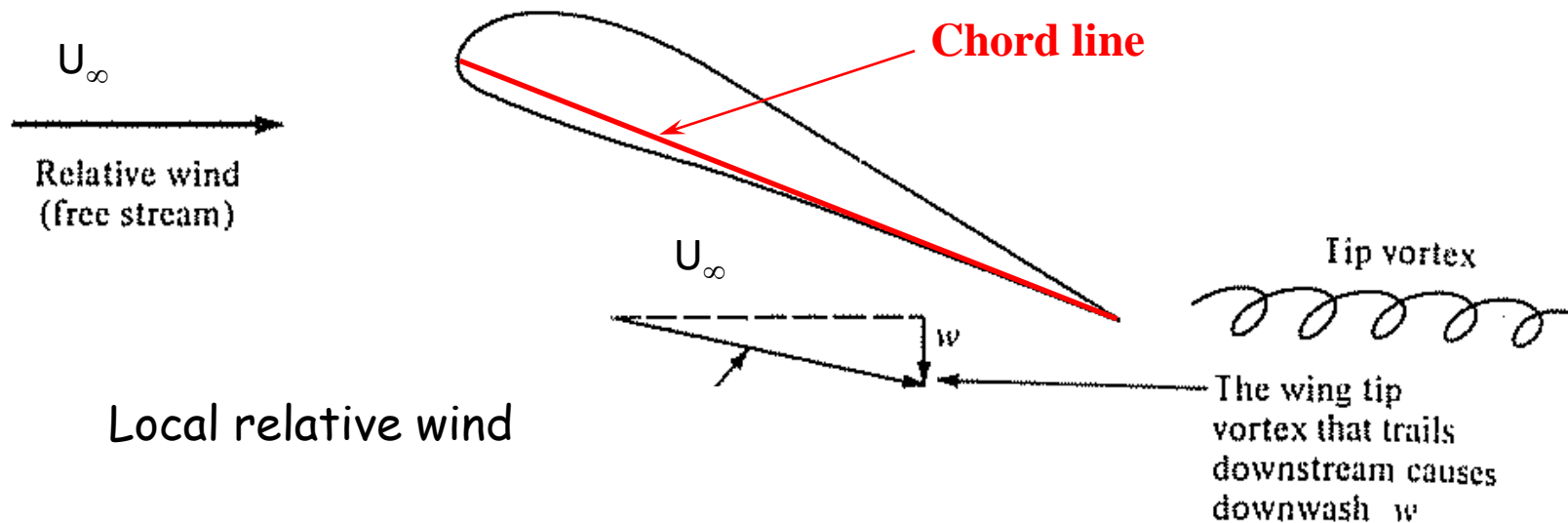
- The downwash velocity component has the effect of “tilting” the undisturbed air, so the effective angle of attack of the airfoil at the aerodynamic center (the quarter chord) is:

$$\alpha_e = \alpha - \varepsilon$$

- The significance of this reduction in the effective angle of attack is that the airfoil section produces less lift and has a new component of drag.
- Since the direction of the resultant velocity at the aerodynamic center is inclined downward, the effective lift of the section of interest is inclined aft by the same amount.
- Therefore, the effective lift on the wing has a component of force parallel to the undisturbed free-stream air which is a drag force.

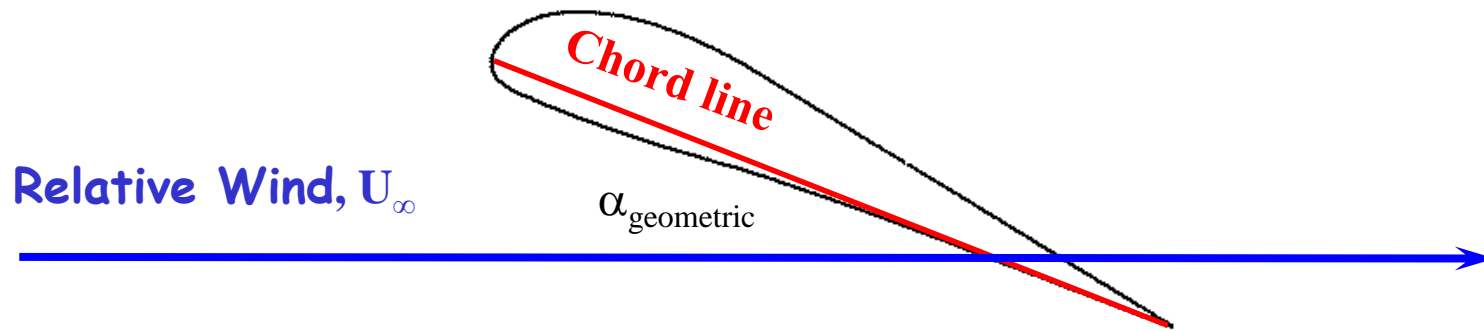
Note: FINITE WING DOWNWASH

- Wing tip vortices induce a small downward component of air velocity near wing by dragging surrounding air with them
- Downward component of velocity is called **downwash, w**



- **Two Consequences:**
 1. Increase in drag, called **induced drag (drag due to lift)**
 2. Angle of attack is effectively reduced, α_{eff} as compared with U_∞

Note: ANGLE OF ATTACK DEFINITIONS

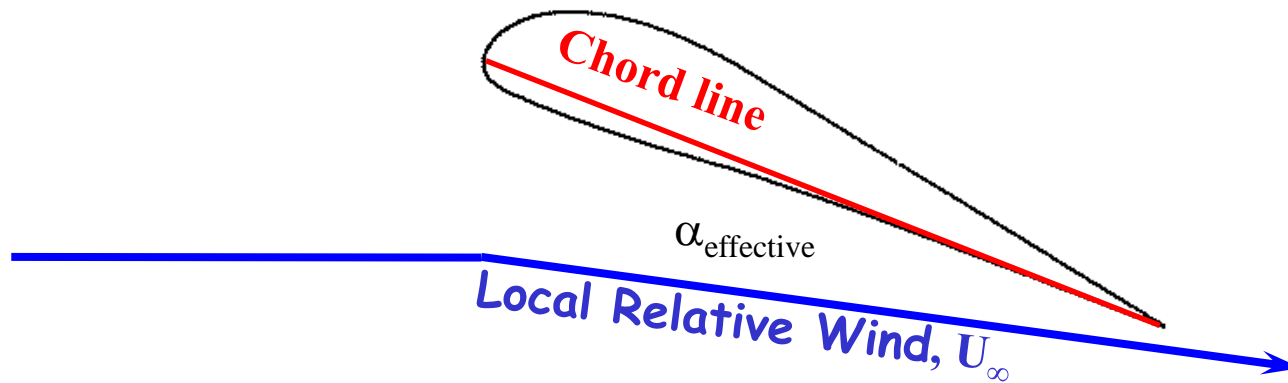


$\alpha_{\text{geometric}}$: what you see, what you would see in a wind tunnel

Simply look at angle between **incoming relative wind** and **chord line**

This is a case of no wing-tips (infinite wing)

Note: ANGLE OF ATTACK DEFINITIONS



$\alpha_{\text{effective}}$: what the airfoil 'sees' locally

Angle between **local flow direction** and **chord line**

Smaller than $\alpha_{\text{geometric}}$ because of downwash

The wing-tips have caused this local relative wind to be angled downward

Note: ANGLE OF ATTACK DEFINITIONS

$$\alpha_{\text{geometric}} = \alpha_{\text{effective}} + \varepsilon$$

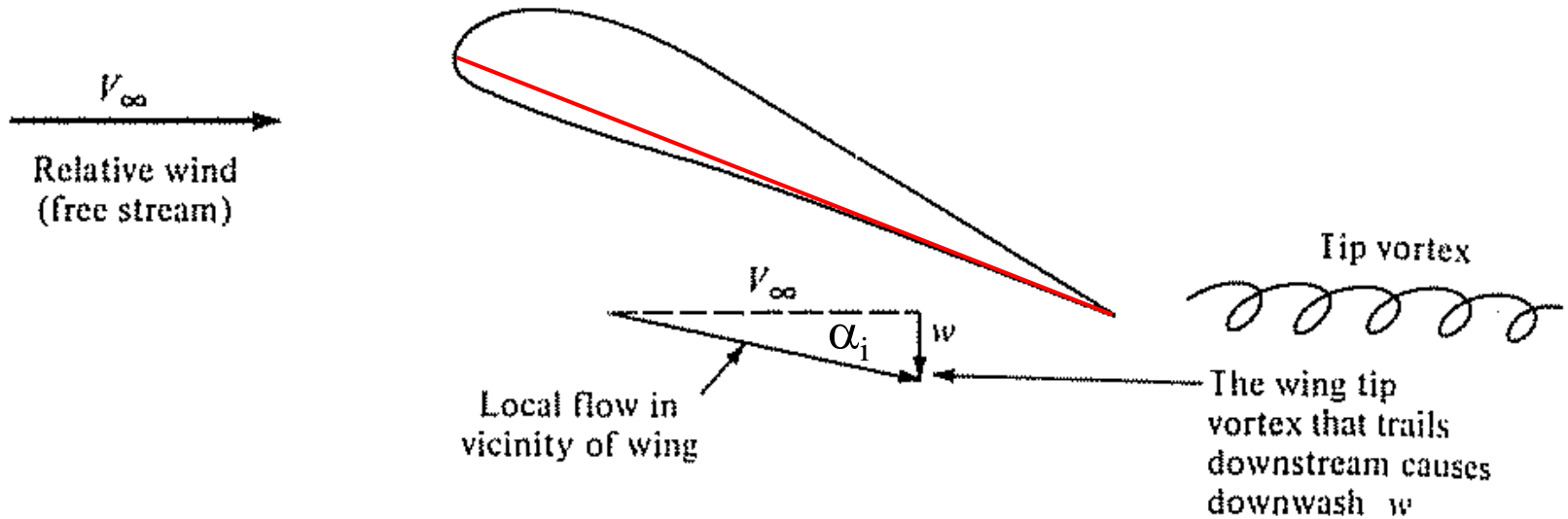
$\alpha_{\text{geometric}}$: what you see, what you would see in a wind tunnel
Simply look at angle between **incoming relative wind** and **chord line**

$\alpha_{\text{effective}}$: what the airfoil 'sees' locally
Angle between local flow direction and chord line
Small than $\alpha_{\text{geometric}}$ because of downwash

(ε): α_{induced} difference between these two angles
Downwash has 'induced' this change in angle of attack

Note: FINITE WING DOWNWASH

- Recall: Wing tip vortices induce a downward component of air velocity near wing by dragging surrounding air with them



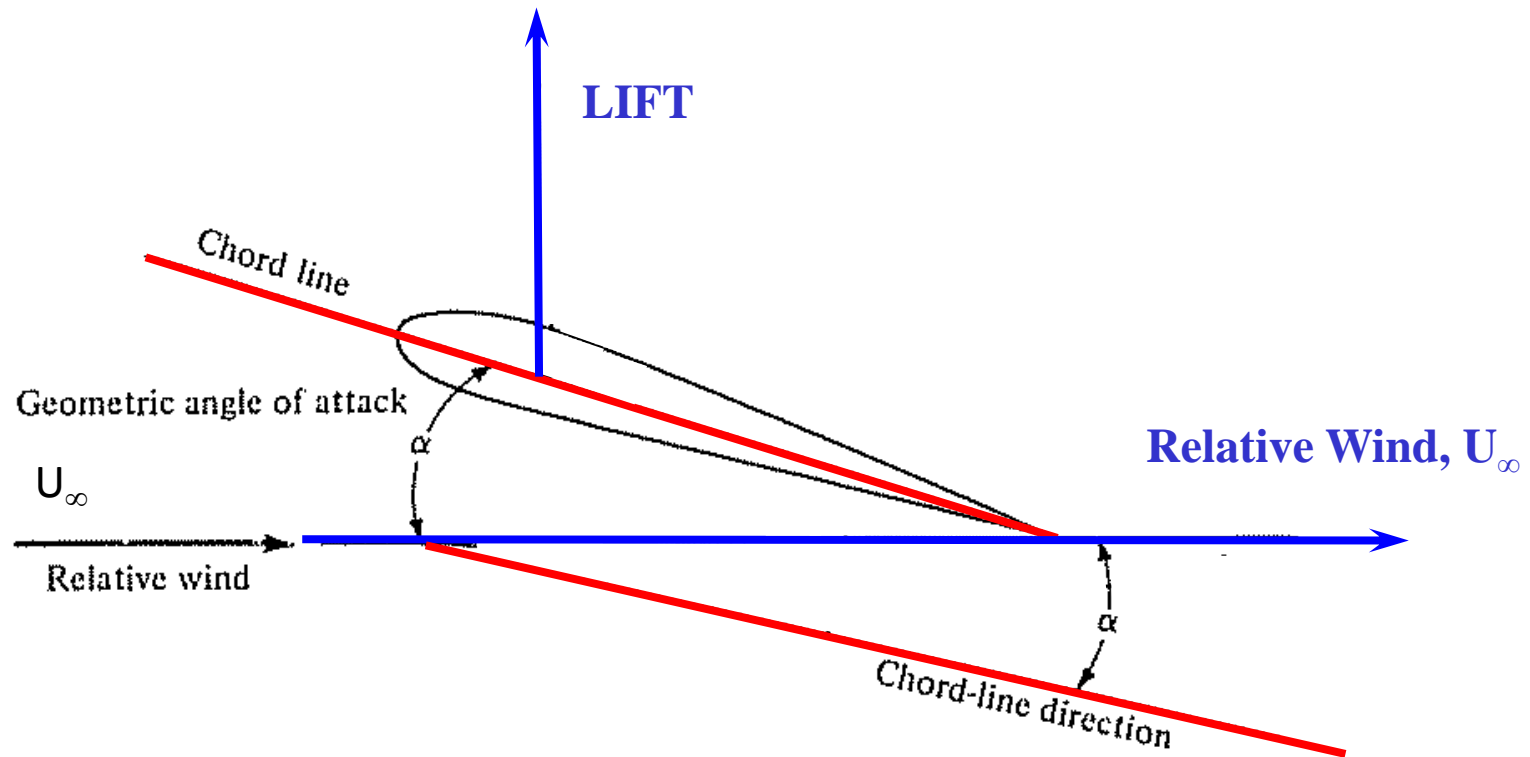
$$\varepsilon(y_1) = \tan^{-1} \left(\frac{-w(y_1)}{U_\infty} \right)$$

$$\varepsilon(y_1) \cong \frac{-w(y_1)}{U_\infty} \quad \text{Small angle}$$

$$\varepsilon(y_1) = \frac{1}{4\pi U_\infty} \int_{-s}^{+s} \left(\frac{d\Gamma}{dy} \right) \frac{dy}{y - y_1}$$

Equation for induced angle of attack along finite wing in terms of $\Gamma(y)$

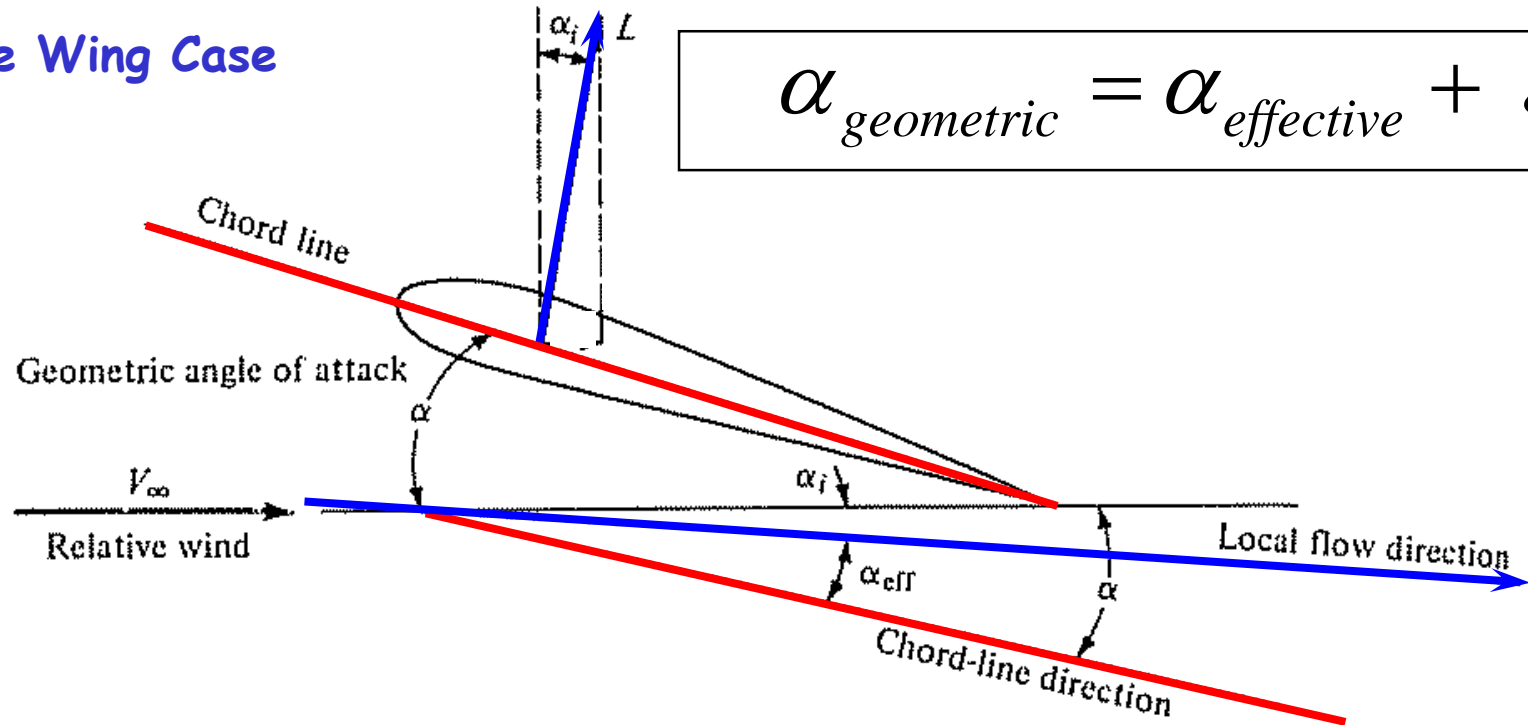
Note: INFINITE WING DESCRIPTION



- LIFT is always perpendicular to the RELATIVE WIND
- All lift is balancing weight

FINITE WING DESCRIPTION

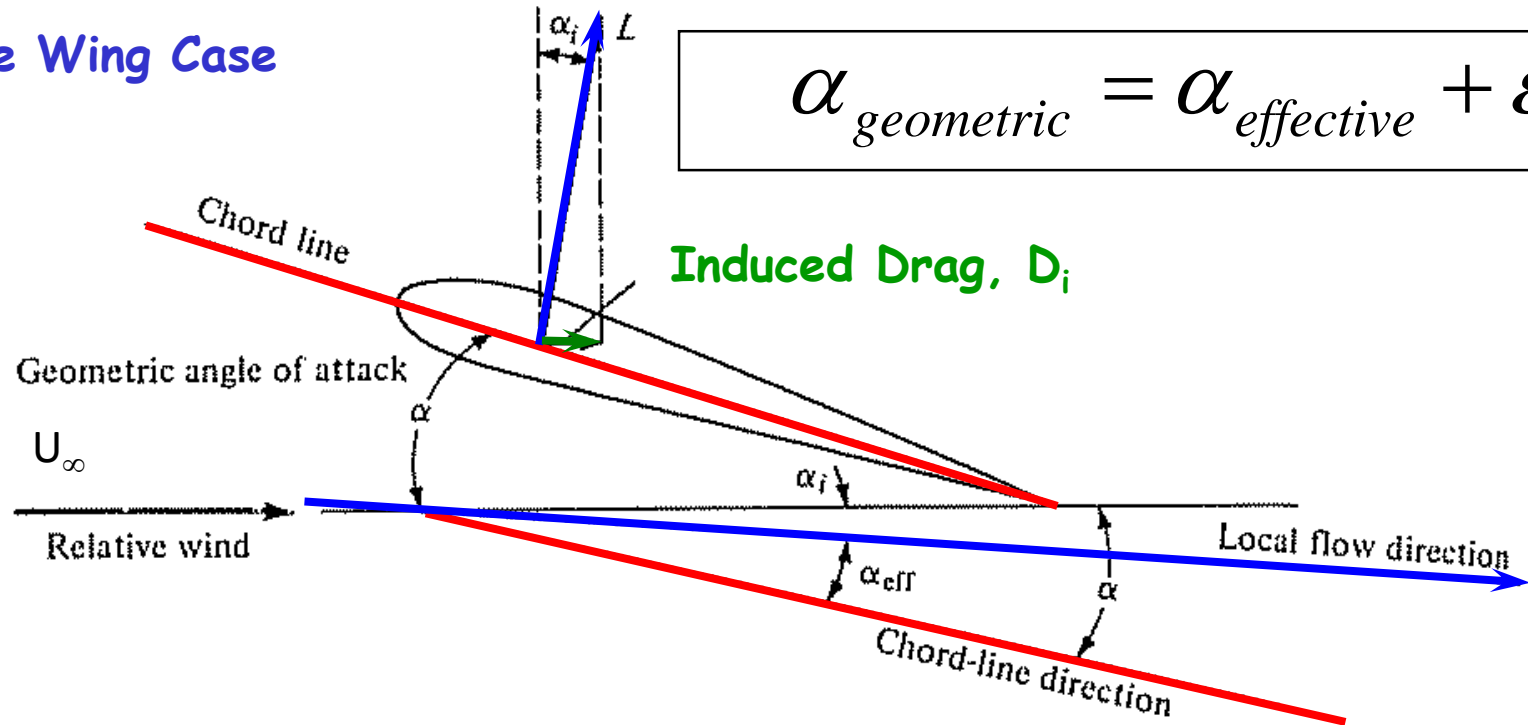
Finite Wing Case



- Relative wind gets tilted downward under the airfoil
- LIFT is still always perpendicular to the RELATIVE WIND

Note: FINITE WING DESCRIPTION

Finite Wing Case



- Drag is measured in direction of *incoming* relative wind (that is the direction that the airplane is flying)
- Lift vector is tilted back
- Component of L acts in direction parallel to *incoming* relative wind → results in a new type of drag

Drag-due-to-lift

- This drag force is a consequence of the lift developed by a finite wing and is termed *vortex drag* (or **the induced drag** or the **drag-due-to-lift**).
- As a result, the lift generated by a finite-span wing composed of a given airfoil section, which is at the geometric angle of attack α_e , is less than that for an infinite-span airfoil composed of the same airfoil section and which is at the same angle of attack α .
- Based on the **Kutta-Joukowski theorem**, the lift on an elemental airfoil section of the wing and the total lift are:

$$l(y) = \rho_{\infty} U_{\infty} \Gamma(y) \rightarrow L = \int^s l(y) dy = \rho_{\infty} U_{\infty} \int^s \Gamma(y) dy$$

- The vortex drag is given using the small angle assumption

$$d_v(y) = l(y) \tan(-w(y)/U_{\infty}) \approx -l(y)w(y)/U_{\infty} = -\rho_{\infty} w(y)\Gamma(y)$$

- The minus sign results because a negative value of **w** produces a positive drag force

drag-due-to-lift

- and the total vortex drag is given by:

$$D_v = -\rho_\infty \int_{-s}^s w(y) \Gamma(y) dy$$

- Notice that for the 2-D airfoil the circulation strength is constant across the span (i.e., it is independent of y) and the induced downwash velocity is zero at all points since there are no trailing vortices.
- Therefore, $D_v = 0$ for a 2-D airfoil.
- As a consequence of the trailing vortex system, the aerodynamic characteristics are modified significantly from those of a two-dimensional airfoil of the same section, which we will now quantify.

Case of Elliptic Span-wise Circulation Distribution

- An especially simple circulation distribution, which also has significant practical implications, is given by the elliptic circulation distribution

$$\Gamma(y) = \Gamma_0 \sqrt{1 - \left(\frac{y}{s}\right)^2} \Rightarrow l(y) = \rho_\infty U_\infty \Gamma_0 \sqrt{1 - \left(\frac{y}{s}\right)^2}$$

- For the elliptic circulation distribution the induced downwash velocity is found from equation

$$w_{y1} = + \frac{1}{4\pi} \int_{-s}^s \frac{d\Gamma / dy}{(y - y_1)} dy \quad \& \quad \frac{d\Gamma}{dy} = - \frac{\Gamma_0}{s^2} \frac{y}{\left(1 - \frac{y^2}{s^2}\right)^{\frac{1}{2}}} \rightarrow$$

$$w_{y1} = - \frac{\Gamma_0}{4\pi s} \int_{-s}^s \frac{y}{\left(s^2 - y^2\right)^{\frac{1}{2}} (y - y_1)} dy$$

$$w_{y1} = - \frac{\Gamma_0}{4\pi s} \left[\int_{-s}^s \frac{(y - y_1) dy}{\left(s^2 - y^2\right)^{\frac{1}{2}} (y - y_1)} + \int_{-s}^s \frac{y_1 dy}{\left(s^2 - y^2\right)^{\frac{1}{2}} (y - y_1)} \right]$$

Note: ELLIPTICAL LIFT DISTRIBUTION

- For a wing with same airfoil shape across span and no twist, an elliptical lift distribution is characteristic of an elliptical wing planform

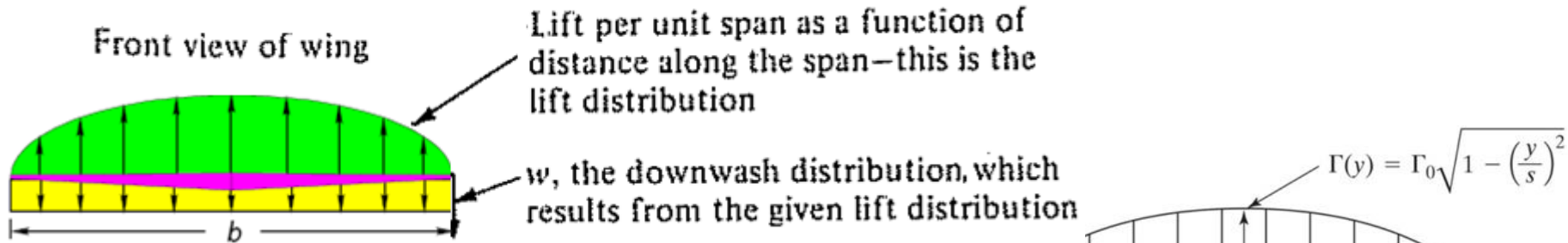


Elliptical Wing Plan-form



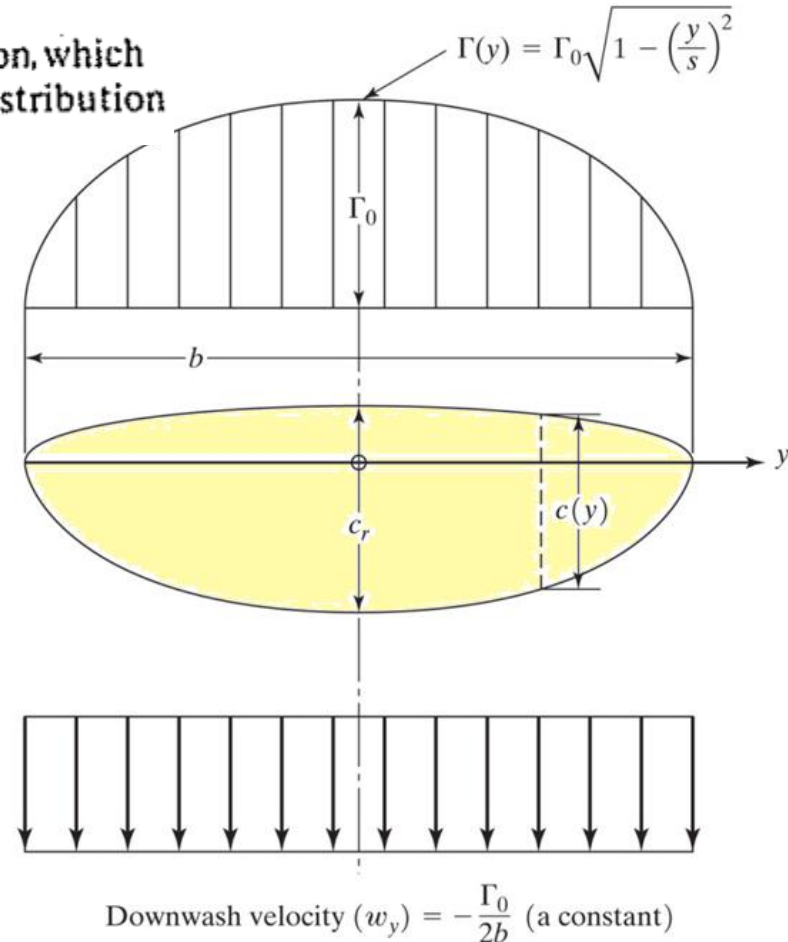
- The Republic P-47 Thunderbolt and Supermarine Spitfire Fighter Aircraft of World War II Both Had Elliptical Wing Plan-forms

Note: Elliptic-circulation distribution and the resultant downwash velocity.



Points to Note:

1. At origin ($y=0$) $\Gamma=\Gamma_0$
2. Circulation varies elliptically with distance y along span
3. At wing tips $\Gamma(-s)=\Gamma(s)=0$
 - Circulation and Lift $\rightarrow 0$ at wing tips



Elliptic Circulation Distribution

- Now we can integrate this expression to obtain:

$$w_{y_1} = -\frac{\Gamma_0}{4\pi s} (\pi + y_1 I) \quad \& \quad I = \int_{-s}^s \frac{dy}{\sqrt{s^2 - y^2} (y - y_1)}$$

- Since the elliptic loading is symmetric about the pitch plane of the vehicle (i.e., $y = 0$), the velocity induced at a point $y_1 = +a$ should be equal to the velocity at a point $y_1 = -a$.
- This can only be true if $I = 0$. Therefore, for the elliptic circulation distribution the downwash is:

$$w_{y_1} = w(y) = -\frac{\Gamma_0}{4s}$$

- which is the very interesting result that the induced velocity is independent of the spanwise position on the wing.
- The total lift for the wing is given by the Kutta-Joukowski theorem as:

$$L = \rho_\infty U_\infty \Gamma_0 \int_{-s}^s \left(1 - \frac{y^2}{s^2}\right)^{\frac{1}{2}} dy$$

Case of Elliptic Spanwise Circulation Distribution

- The lift equation can be made easier to integrate by using the coordinate transformation:

$$y = -s \cos \phi \quad dy = s \sin \phi \, d\phi$$

- where the left wing tip corresponds to $\phi = 0$ and the right wing tip corresponds to $\phi = \pi$, resulting in:

This expression can now be integrated to find:

$$L = \rho_{\infty} U_{\infty} \Gamma_0 \int_0^{\pi} \sqrt{1 - \left(\frac{-s \cos \phi}{s}\right)^2} s \sin \phi \, d\phi = \rho_{\infty} U_{\infty} \Gamma_0 \int_0^{\pi} \sqrt{1 - \cos^2 \phi} s \sin \phi \, d\phi$$

- and the lift coefficient for the wing is:

$$L = \rho_{\infty} U_{\infty} \Gamma_0 s \frac{\pi}{2} = \frac{\pi}{4} b \rho_{\infty} U_{\infty} \Gamma_0$$

$$C_L = \frac{L}{\frac{1}{2} \rho_{\infty} U_{\infty}^2 S} = \frac{\frac{\pi}{4} b \rho_{\infty} U_{\infty} \Gamma_0}{\frac{1}{2} \rho_{\infty} U_{\infty}^2 S} = \frac{\pi b \Gamma_0}{2 U_{\infty} S}$$

- From this equation, we can find the mid-span circulation as:

$$\Gamma_0 = \frac{2C_L U_\infty S}{\pi b}$$

- We can also find the downwash angle since:

$$\varepsilon = \frac{-w}{U_\infty} = + \frac{\Gamma_0}{4U_\infty s} = \frac{\Gamma_0}{2U_\infty b}$$

- The downwash angle is constant along the span of the wing.

$$\varepsilon = \frac{\Gamma_0}{2U_\infty b} = \frac{2C_L U_\infty S}{2U_\infty b \pi b} = \frac{C_L S}{\pi b^2} = \frac{C_L}{\pi AR}$$

- Introducing the coordinate transformation again, we obtain:

$$D_v = -\rho_\infty \int_{-s}^s w(y) \Gamma(y) dy = -\rho_\infty \int_{-s}^s \frac{\Gamma_0}{4s} \Gamma_0 \sqrt{1 - \left(\frac{y}{s}\right)^2} dy$$

Elliptic Spanwise Circulation Distribution

$$D_v = \rho_\infty \frac{\Gamma_0^2}{4S} \int_0^\pi \sqrt{1 - \cos^2 \phi} s \sin \phi d\phi = \frac{\pi}{8} \rho_\infty \Gamma_0^2$$

- and the drag coefficient for the induced component is

$$C_{Dv} = \frac{D_v}{\frac{1}{2} \rho_\infty U_\infty^2 S} = \frac{\frac{\pi}{8} \rho_\infty \Gamma_0^2}{\frac{1}{2} \rho_\infty U_\infty^2 S} = \frac{\pi \Gamma_0^2}{4 U_\infty^2 S}$$

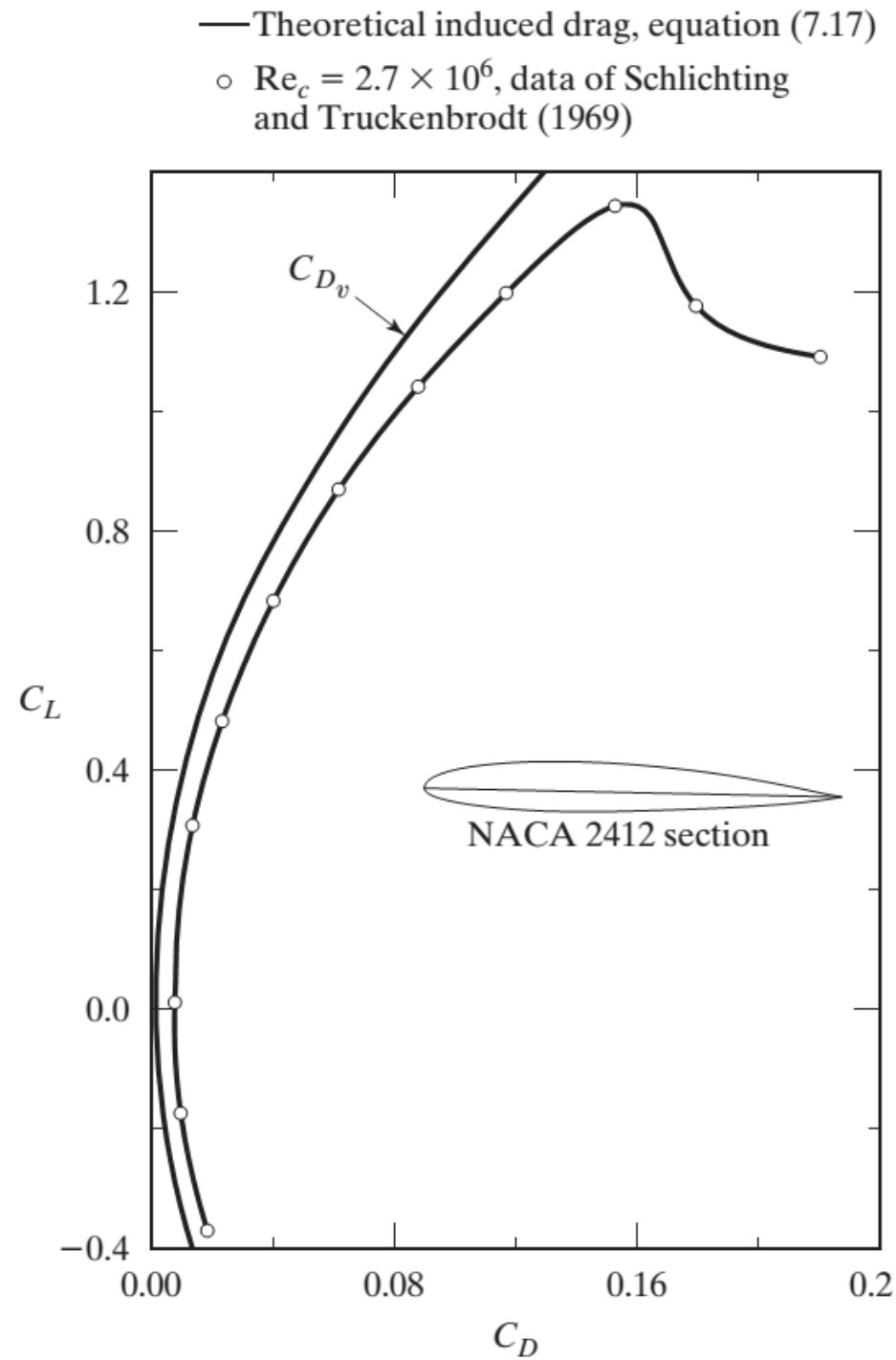
- Using the relation for Γ_0 , the vortex drag coefficient becomes:

- The induced drag is zero for a $C_L = 0$ airfoil (i.e., a wing with an aspect ratio (AR) of infinity).

$$C_{Dv} = \frac{\pi 4 C_L^2 U_\infty^2 S^2}{4 U_\infty^2 S \pi^2 b^2} = \frac{C_L^2 S}{\pi b^2} = \frac{C_L^2}{\pi AR}$$

Comparison with Experiments

- Experimental drag polar for a wing with an aspect ratio of $AR=5$ compared with the theoretical induced drag



Comparison with Experiments

- The induced drag coefficient given by equation and the measurements for a wing whose aspect ratio is 5 are compared.
- The experimental values of the induced drag coefficient closely follow the theoretical values up to an angle of attack of 20°.
- The relatively constant difference between the measured values and the theoretical values is due to the influence of skin friction, which was not included in the development.
- Therefore the drag coefficient for an incompressible flow is typically written as:
 - where C_{D0} is the drag coefficient at zero lift and kC_L^2 is the lift-dependent drag coefficient.
- The lift-dependent drag coefficient includes that part of the viscous drag and of the form drag, which results as the angle of attack changes from α_{0f} .

$$C_D = C_{D0} + kC_L^2$$

EXAMPLE 7.1: Lift and vortex drag coefficients for a wing with an elliptic lift distribution

The Cessna 172 aircraft has a wing geometry described in Table 5.1, a wing area of 174 ft^2 , and a gross weight of 2450 pounds. If the airplane is flying at 100 miles per hour on a standard day at sea level, find the lift and vortex drag coefficients assuming the wing has an elliptic lift distribution and all of the lift is generated by the wing.

Solution: The velocity of the airplane is given in miles per hour and needs to be converted to feet per second in order to use consistent units.

$$U_\infty = (100 \text{ mile/h})(5280 \text{ ft/mile}) / (3600 \text{ s/h}) = 146.7 \text{ ft/s}$$

The lift coefficient is found assuming the aircraft is flying in SLUF conditions where $L = W$. The lift coefficient can then be found from:

$$C_L = \frac{L}{\frac{1}{2}\rho_\infty U_\infty^2 S} = \frac{W}{\frac{1}{2}\rho_\infty U_\infty^2 S} = \frac{2450 \text{ lb}}{\frac{1}{2}(0.002377 \text{ slug/ft}^3)(146.7 \text{ ft/s})^2(174 \text{ ft}^2)} = 0.551$$

From Table 5.1 the aspect ratio of the Cessna 172 is given as 7.32. Using equation (7.17) the vortex drag coefficient for an elliptic lift distribution is:

$$C_{Dv} = \frac{C_L^2}{\pi AR} = \frac{(0.551)^2}{7.32\pi} = 0.0132$$

Technique for General Spanwise Circulation Distribution

- Consider a spanwise circulation distribution that can be represented by a Fourier sine series consisting of N terms:

$$\Gamma(\phi) = 4sU_{\infty} \sum_1^N A_n \sin n\phi$$

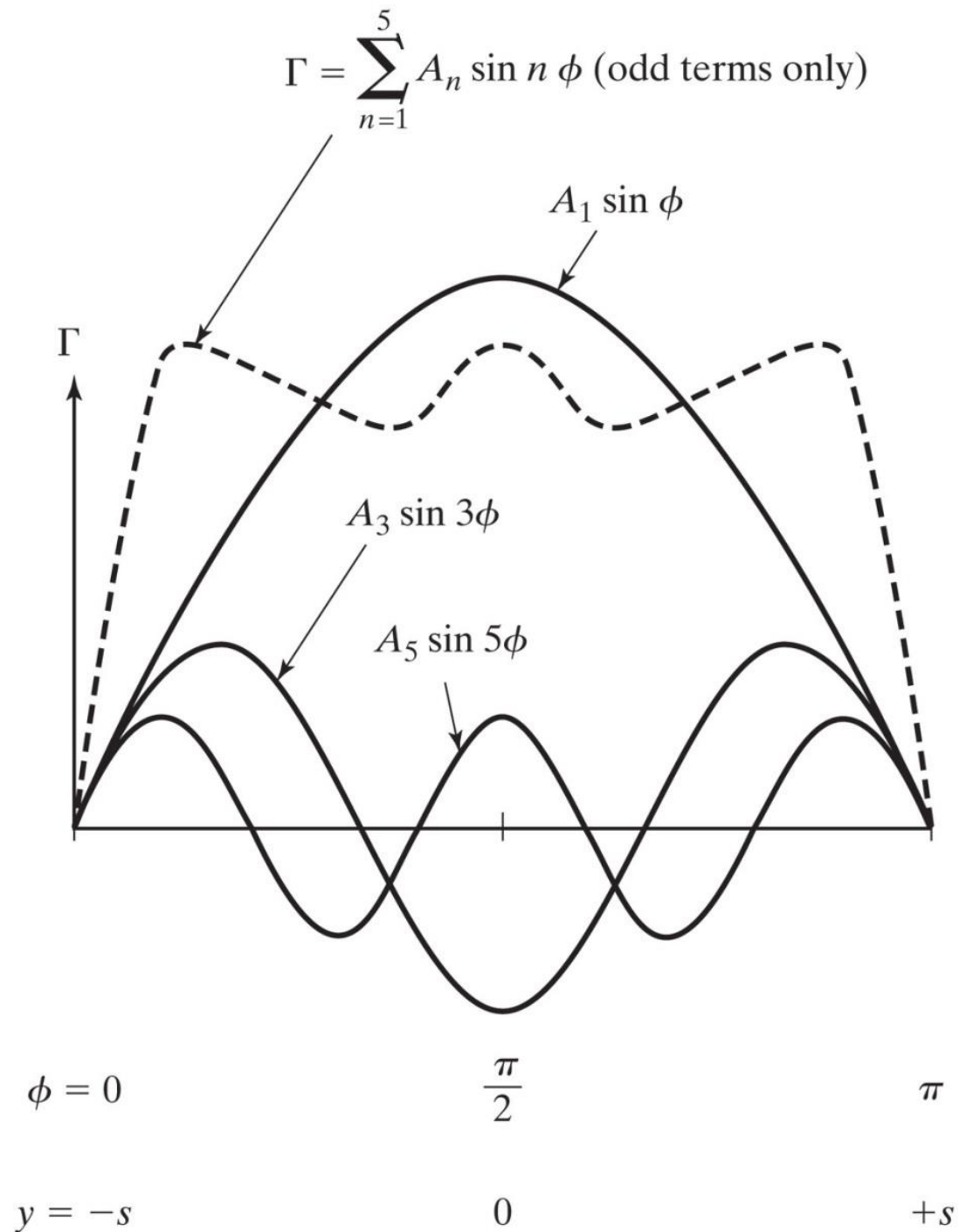
- The spanwise coordinate (y) has been replaced by the ϕ coordinate:

$$y = -s \cos\phi$$

- A sketch of one such Fourier series is presented on next slide.
- Since the spanwise lift distribution represented is symmetrical, only the odd terms remain.
- The section lift force is found by applying the **Kutta-Joukowski** theorem:

$$l(\phi) = \rho_{\infty} U_{\infty} \Gamma(\phi) = 4s\rho_{\infty} U_{\infty}^2 \sum_1^N A_n \sin n\phi$$

Symmetric spanwise lift distribution as represented by a sine series.



- To evaluate the coefficients $A_1, A_2, A_3, \dots, A_N$, it is necessary to determine the circulation at N spanwise locations.
- the N -resultant linear equations can be solved for the A_N coefficients.
- The series is truncated to a finite series and the coefficients in the finite series are evaluated by requiring the lifting-line equation to be satisfied at a number of spanwise locations equal to the number of terms in the series.
- This method is known as the **collocation method**.
- Recall that the section lift coefficient is defined as

$$C_l(\phi) = \frac{\text{lift per unit span}}{\frac{1}{2} \rho_\infty U_\infty^2 c}$$

- Using the local circulation to determine the local lift per unit span, we obtain

$$C_l(\phi) = \frac{\rho_\infty U_\infty \Gamma(\phi)}{\frac{1}{2} \rho_\infty U_\infty^2 c} = \frac{2\Gamma(\phi)}{U_\infty c}$$

General Spanwise Circulation Distribution

- It is also possible to evaluate the section lift coefficient by using the linear correlation between the lift and the angle of attack for the equivalent 2-D flow.

$$C_l = \left(\frac{dC_l}{d\alpha} \right)_0 (\alpha_e - \alpha_{0l})$$

- We now have two expressions for calculating the section lift coefficient at a particular spanwise location ϕ .
- We equate the two expressions to form an important equation
- Let the equivalent lift-curve slope $(dC_l/d\alpha)_0$ be designated by the symbol a_0 .
- Since $\alpha_e = \alpha - \varepsilon$, the two equations can be combined to yield the relation:

$$\frac{2\Gamma(\phi)}{c(\phi)a_0} = U_\infty [\alpha(\phi) - \alpha_{0l}(\phi)] - U_\infty \varepsilon(\phi) \quad 7.25$$

- Note that five parameters in the equation may depend on the spanwise location ϕ (or y) at which we will evaluate the terms.
- The five parameters are:
 1. Γ , the local circulation;
 2. ε , the downwash angle, which depends on the circulation distribution;
 3. c , the chord length, which varies with ϕ for a tapered wing planform;
 4. α , the local geometric angle of attack, which varies with ϕ when the wing is twisted; and
 5. α_{0l} , the zero lift angle of attack, which varies with ϕ when the airfoil section varies in the spanwise direction (*aerodynamic twist*).

Using equation (7.3), we can find the induced angle of attack in terms of the downwash velocity as:

$$U_{\infty} \varepsilon = -w = -\frac{1}{4\pi} \int_{-s}^{+s} \frac{d\Gamma / dy}{y - y_1} dy$$

General Spanwise Circulation Distribution

- Using the Fourier series representation for Γ and the coordinate transformation, we obtain:

$$-w = U_\infty \varepsilon = U_\infty \frac{\sum nA_n \sin n\phi}{\sin \phi} \Rightarrow \varepsilon = -\frac{w}{U_\infty} = \frac{\sum nA_n \sin n\phi}{\sin \phi}$$

- Equation (7.25) can now be rewritten using the above relation:

$$\frac{2\Gamma}{ca_0} = U_\infty [\alpha - \alpha_{0l}] - U_\infty \frac{\sum nA_n \sin n\phi}{\sin \phi}$$

, the equation becomes:

- Since

$$\Gamma(\phi) = 4sU_\infty \sum_1^N A_n \sin n\phi$$

$$\frac{8s}{ca_0} \sum A_n \sin n\phi = (\alpha - \alpha_{0l}) - \frac{\sum nA_n \sin n\phi}{\sin \phi}$$

Technique for General Spanwise Circulation Distribution

- Defining $\mu = c_{\infty}/8s$, the resultant governing equation is:

$$\mu(\alpha - \alpha_{0l}) \sin \phi = \sum A_n \sin n\phi (\mu n + \sin \phi)$$

- which is known as the *monoplane equation*.
- If we consider only symmetrical loading distributions, only the odd terms of the series need to be considered.

$$\Gamma(\phi) = 4sU_{\infty} (A_1 \sin \phi + A_3 \sin 3\phi + A_5 \sin 5\phi + \dots)$$

Lift on the Wing

- The lift on the wing can now be found using equation (7.22):

$$L = \int_{-s}^{+s} \rho_{\infty} U_{\infty} \Gamma(y) dy = \int_0^{\pi} \rho_{\infty} U_{\infty} s \Gamma(\phi) \sin \phi d\phi$$

- Using the Fourier series for $\Gamma(\phi)$ we find that:

$$L = 4\rho_{\infty} U_{\infty}^2 s^2 \int_0^{\pi} \sum A_n \sin n\phi \sin \phi d\phi$$

- Noting that $\sin A \sin B = \frac{1}{2} \cos(A - B) - \frac{1}{2} \cos(A + B)$, the integration yields

The summation ~~represented by the second term is zero, since each of the terms is zero for $n \neq 1$~~

$$4\rho_{\infty} U_{\infty}^2 s^2 \left\{ A_1 \left[\frac{\phi}{2} + \frac{\sin 2\phi}{4} \right]_0^{\pi} + \sum_3 \frac{1}{2} A_n \left[\frac{\sin(n-1)\phi}{n-1} - \frac{\sin(n+1)\phi}{n+1} \right]_0^{\pi} \right\}$$

Lift on the Wing

- Therefore, the integral expression for the lift becomes:

$$L = 4(s^2) \left(\frac{1}{2} \rho_{\infty} U_{\infty}^2 \right) A_1 \pi = C_L \left(\frac{1}{2} \rho_{\infty} U_{\infty}^2 \right) (S)$$

- and the wing lift coefficient is:

$$C_L = A_1 \pi AR$$

- The lift depends only on the magnitude of the first coefficient, no matter how many terms may be present in the series describing the distribution
- Note that local lift coefficient is:

$$C_l(\phi) = \frac{2\Gamma(\phi)}{U_{\infty}c}$$

Vortex-Induced Drag

- The vortex-induced drag can also be found.

$$\begin{aligned} D_v &= - \int_{-s}^{+s} \rho_\infty w \Gamma dy \\ &= \rho_\infty \int_0^\pi \underbrace{\frac{U_\infty \sum n A_n \sin n\phi}{\sin \phi}}_{-w} \underbrace{4s U_\infty \sum A_n \sin n\phi}_{\Gamma} \underbrace{s \sin \phi}_{dy} d\phi \\ &= 4\rho_\infty s^2 U_\infty^2 \int_0^\pi \sum n A_n \sin n\phi \sum A_n \sin n\phi d\phi \end{aligned}$$

- The integral can be evaluated as:

$$\int_0^\pi \sum n A_n \sin n\phi \sum A_n \sin n\phi d\phi = \frac{\pi}{2} \sum n A_n^2$$

Vortex-Induced Drag

- So, the coefficient for the vortex-induced drag is:

$$C_{Dv} = \pi \cdot AR \sum n A_n^2$$

- Since $A_1 = C_L / (\pi AR)$, we can re-write the equation as

$$C_{Dv} = \frac{C_L^2}{\pi \cdot AR} \sum n \left(\frac{A_n}{A_1} \right)^2$$

- where only the odd terms in the series are considered for a symmetric lift distribution ($n = 1, 3, 5, \dots$).

$$C_{Dv} = \frac{C_L^2}{\pi \cdot AR} \left[1 + \left(\frac{3A_3^2}{A_1^2} + \frac{5A_5^2}{A_1^2} + \frac{7A_7^2}{A_1^2} + \dots \right) \right]$$

$$C_{Dv} = \frac{C_L^2}{\pi \cdot AR} (1 + \delta) = \frac{C_L^2}{\pi e \cdot AR}$$

Vortex-Induced Drag

- where e is the **span efficiency factor of the wing** and $e = 1 / (1 + \delta)$.
- Typical values for the span efficiency factor range between 0.6 and 0.95, with $e = 1$ being the value for an elliptic lift distribution.
- In general, values of e should be as close to $e = 1$ as possible to improve the aerodynamic efficiency of the wing.
- The induced drag factor δ is given by:

$$\delta = \frac{3A_3^2}{A_1^2} + \frac{5A_5^2}{A_1^2} + \frac{7A_7^2}{A_1^2} + \dots$$

- which is the elliptic distribution.
- The effect of the taper ratio on the spanwise variation of the lift coefficient is illustrated in Fig. 7.13 .
- Theoretical solutions are presented for untwisted wings having taper ratios from 0 to 1.
- The wings, which were composed of NACA 2412 airfoil sections, all had an aspect ratio of 7.28.

Effect of taper ratio

- The local lift coefficient has been divided by the overall lift coefficient for the wings according to:

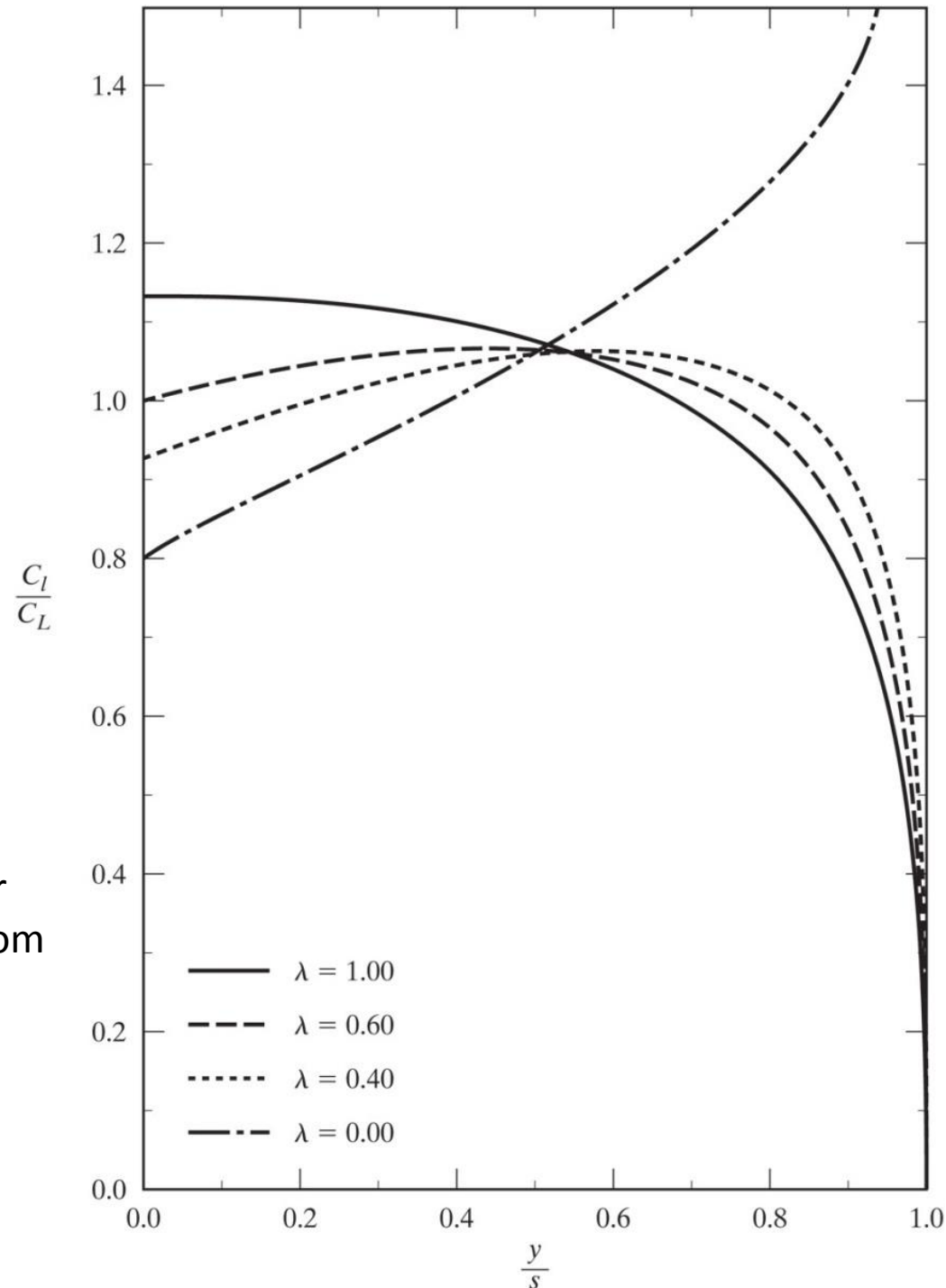
$$\frac{C_l}{C_L} = \frac{2\Gamma / U_\infty c}{\pi A_1 AR} = \frac{2\Gamma / U_\infty c}{\pi A_1 \frac{2b}{(\lambda + 1)c_r}} = \frac{\Gamma(\lambda + 1)c_r}{\pi A_1 U_\infty c(2s)}$$

$$\frac{C_l}{C_L} = \frac{2(1 + \lambda)}{\pi A_1} \frac{c_r}{c(\phi)} \sum \{A_{2n-1} \sin[(2n - 1)\phi]\}$$

- The values of the local (or section) lift coefficient near the tip of the highly tapered wings are significantly greater than the overall lift coefficient for that planform.
- This result is important relative to the separation (or stall) of the boundary layer for a particular planform when it is operating at a relatively high angle of attack, since a highly loaded tip will stall first, placing any ailerons in the unsteady flow field downstream of the stall region

7.13- Effect of taper ratio on the spanwise variation of the lift coefficient for an untwisted wing.

- Theoretical solutions are presented for untwisted wings having taper ratios from 0 to 1.
- The wings, which were composed of NACA 2412 airfoil sections, all had an aspect ratio of 7.28.



Change in the wing lift-curve slope.

- Lifting-line theory can also predict the change in the wing lift-curve slope.
- Since each airfoil section is “seeing” an effective angle of attack which is less than the geometric angle of attack, the lift of the wing is reduced.
- The geometric angle of attack is given by $\alpha = \alpha_e + \varepsilon$, the downwash angle for an elliptic lift distribution is $\varepsilon = C_L/\pi AR$, then the geometric angle of attack for an elliptic lift distribution is:

$$\alpha = \alpha_e + \frac{C_L}{\pi AR}$$

- Taking the derivative of this equation with respect to the lift coefficient:

$$\frac{1}{\alpha} = \frac{1}{\alpha_0} + \frac{1}{\pi AR}$$

Change in the wing lift-curve slope.

- which can be re-arranged to obtain:

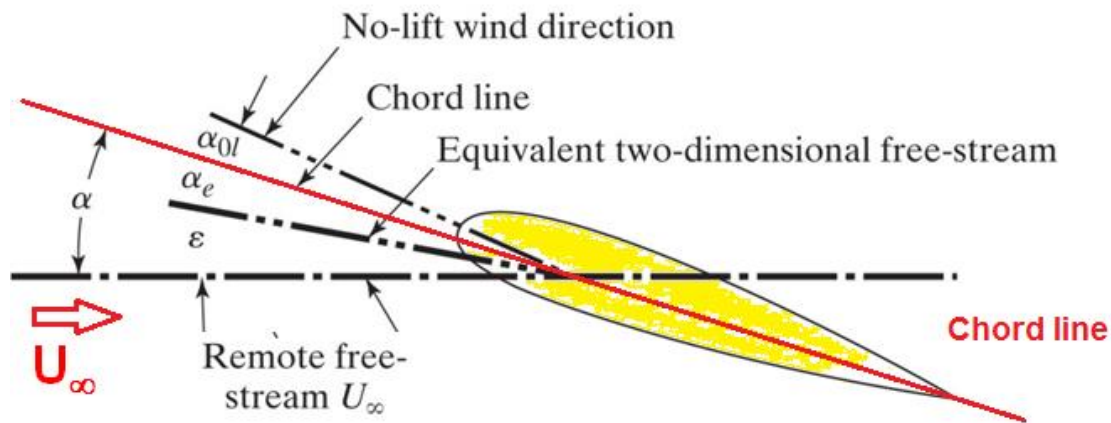
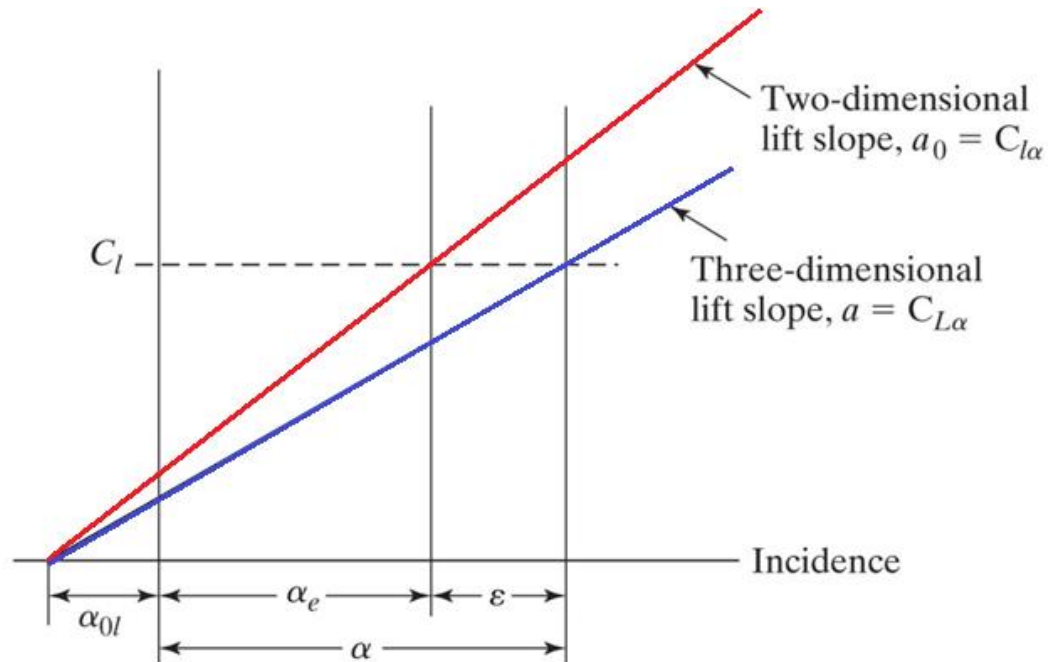
$$a = C_{L_\alpha} = \frac{a_0}{1 + \frac{a_0}{\pi AR}} = \frac{C_{l_\alpha}}{1 + \frac{C_{l_\alpha}}{\pi AR}}$$

- This is the lift-curve slope for a wing with an elliptic lift distribution, which can be extended to a general lift distribution in a similar fashion to the induced drag in equation (7.29) by the addition of a lift-curve slope parameter, τ

$$a = C_{L_\alpha} = \frac{a_0}{1 + \frac{a_0}{\pi AR} (1 + \tau)}$$

- The slope parameter can be obtained from the Fourier coefficients in a similar fashion to δ , but it is common to show the parameter graphically.

Nomenclature for wing/airfoil lift.



Induced drag as a function of taper ratio.

- Fig. 7.14 a shows the induced drag parameter, δ , for planar wings with non-elliptic lift distributions as a function of taper ratio and aspect ratio, and Fig. 7.14 b shows the slope parameter, τ .
- Notice that both parameters have high values at low taper ratios (pointed wing tips) as well as fairly high values at high taper ratios (rectangular wings).
- Each parameter is minimized (and the impact of the wing on induced drag and lift-curve slope reduction is minimized) when the taper ratio is $\lambda = 0.3 - 0.4$.
- A trapezoidal wing with this taper ratio approximates an elliptic planform shape and gives the best results for lift and drag.

Figure 7.14a Effect of aspect ratio and taper ratio on: induced drag parameter.

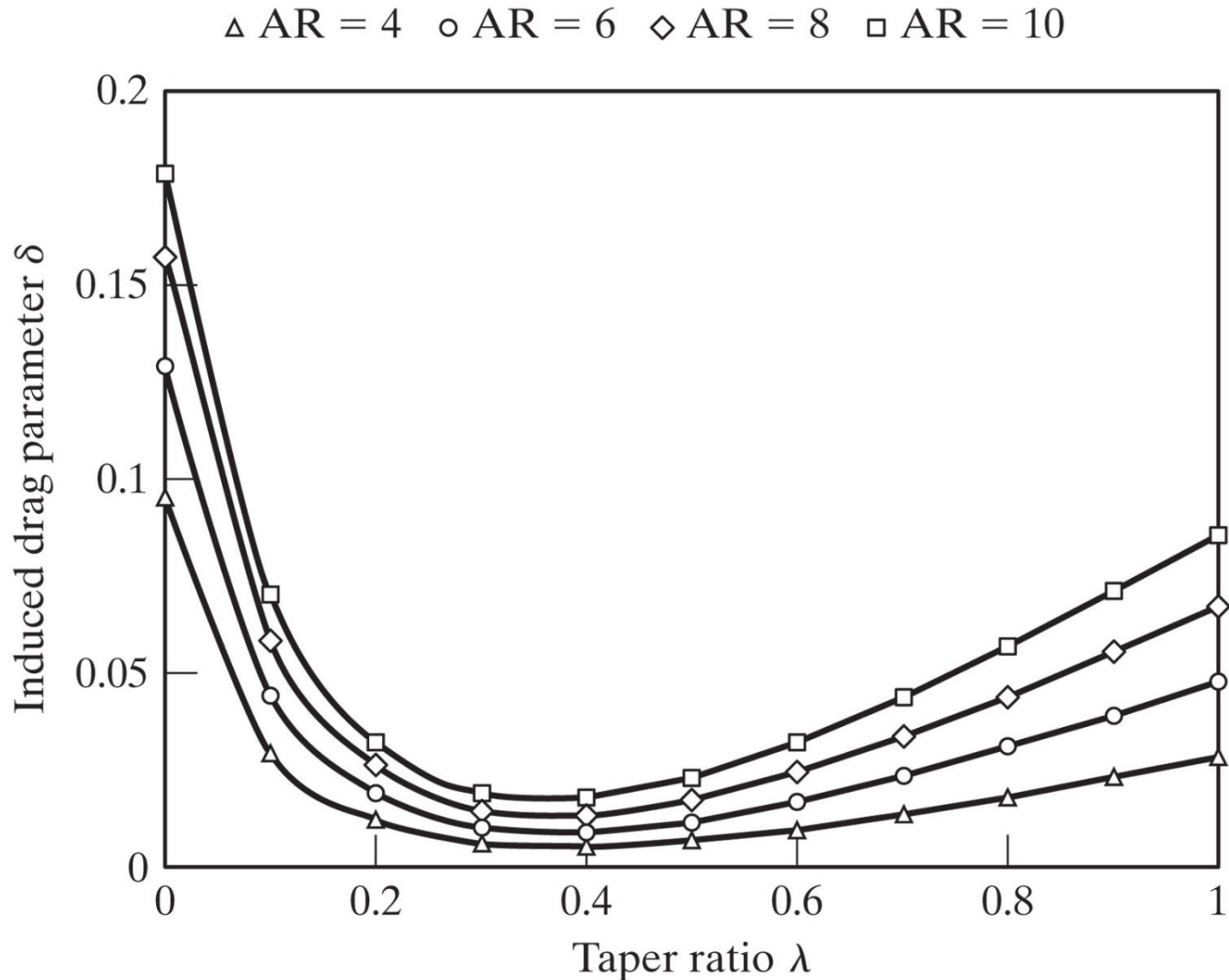
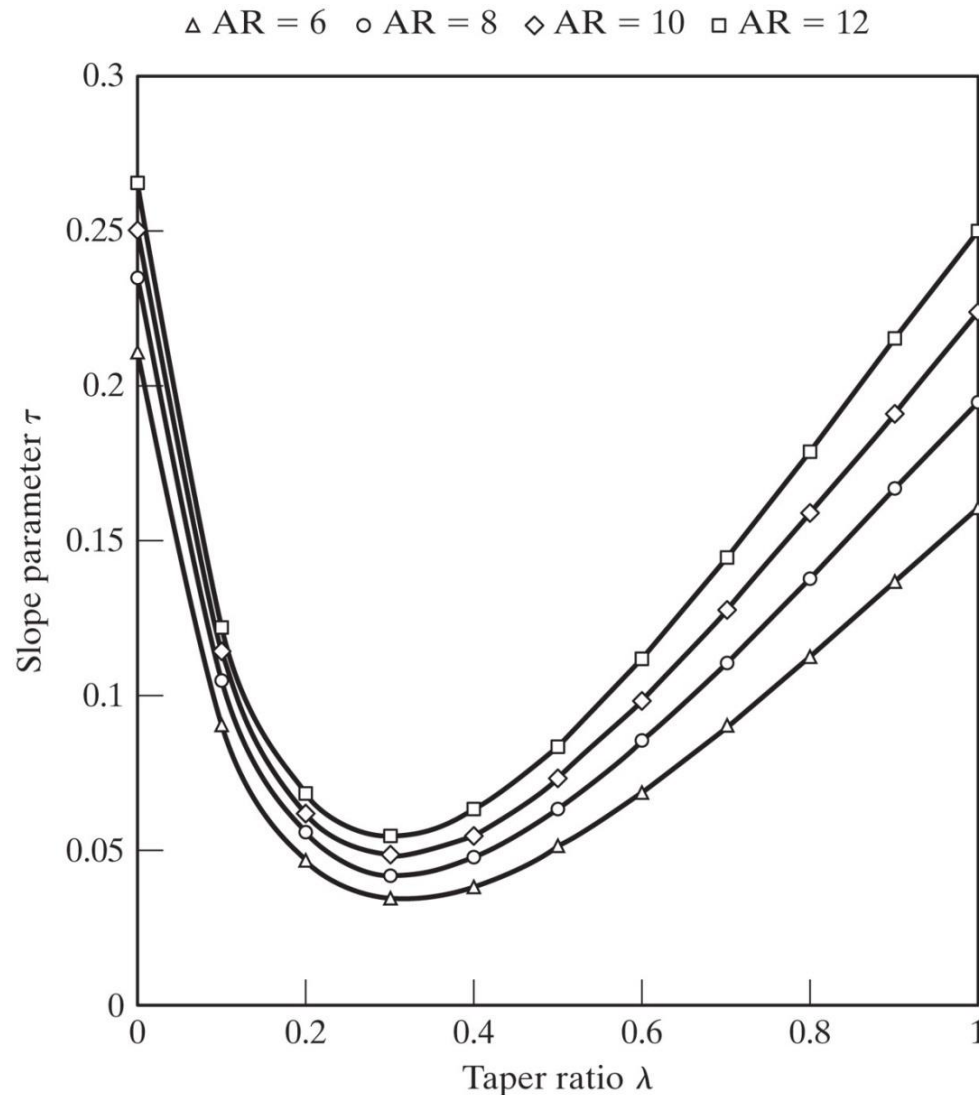


Figure 7.14b Effect of aspect ratio and taper ratio on: lift-curve slope parameter. Airfoil lift-curve slope is assumed to be $2\pi/\text{rad}$.



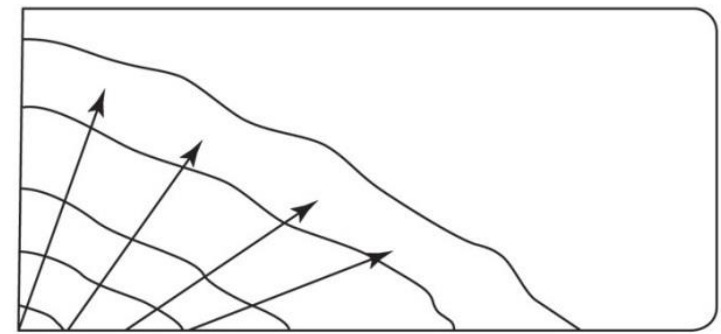
- Once the local lift coefficient reaches the stall angle of attack of the airfoil section, the local airfoil will be stalled, creating a region of flow separation in that vicinity.
- As the angle of attack is further increased, stall patterns will form on the wing, depending on the local lift coefficient variation along the span.
- Sketches of stall patterns are presented in Fig. 7.15.
- The desirable stall pattern for a wing is a stall which begins at the root sections so that the ailerons remain effective at high angles of attack.
- The spanwise load distribution for a rectangular wing indicates stall will begin at the root and proceed outward, which is a favorable stall pattern.
- The spanwise load distribution for a wing with a moderate taper ratio ($\lambda = 0.4$) approximates that of an elliptical wing (i.e., the local lift coefficient is roughly constant across the span).
- As a result, all sections will reach stall at essentially the same angle of attack.

Figure 7.15 Typical stall patterns:

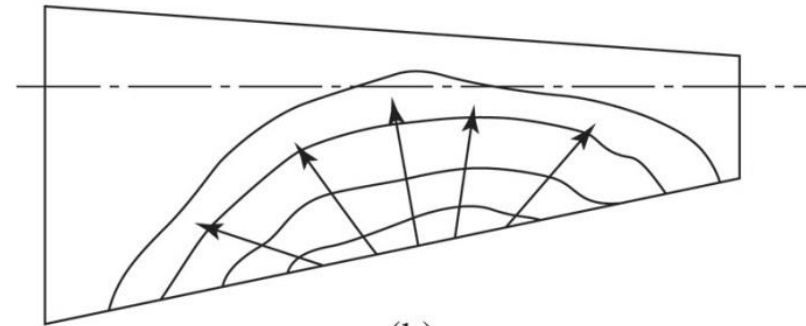
(a) rectangular wing, $\lambda = 1.0$;

(b) moderately tapered wing, $\lambda = 0.4$;

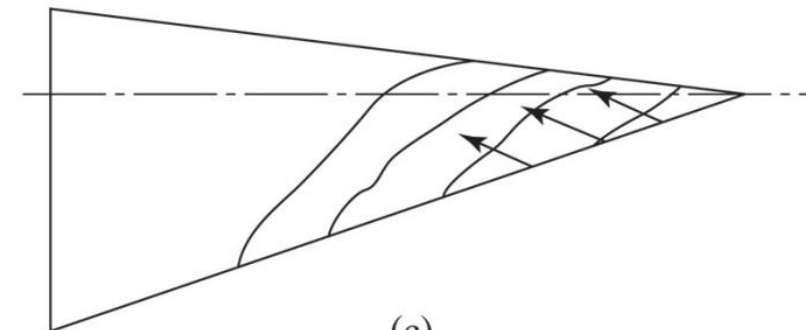
(c) pointed wing, $\lambda = 0.0$.



(a)



(b)



(c)

- Tapering of the wing also reduces the wing-root bending moments, since the inboard portion of the wing carries more of the wing's lift than the tip.
- Furthermore, the longer wing-root chord makes it possible to increase the actual thickness of the wing while maintaining a low thickness ratio, which is needed if the airplane is to operate at high speeds also.
- While taper reduces the actual loads carried outboard, the lift coefficients near the tip are higher than those near the root for a tapered wing.
- Therefore, there is a strong tendency to stall near (or at) the tip for highly tapered (or pointed) wings.
- In order to prevent the stall pattern from beginning in the region of the ailerons, the wing may be given a geometric twist, or washout, to decrease the local angles of attack at the tip.
- The addition of leading-edge slots or slats toward the tip increases the stall angle of attack and is useful in avoiding tip stall and the loss of aileron effectiveness.

EXAMPLE 7.2: Use the monoplane equation to compute the aerodynamic coefficients for a wing

The monoplane equation [i.e., equation (7.26)] will be used to compute the aerodynamic coefficients of a wing for which aerodynamic data are available. The geometry of the wing to be studied is illustrated in Fig. 7.16. The wing, which is unswept at the quarter chord, is composed of NACA 65–210 airfoil sections. Referring to the data of Abbott and von Doenhoff (1949), the zero-lift angle of attack (α_{0l}) for this airfoil is approximately -1.2° across the span. Since the wing is untwisted, the geometric angle of

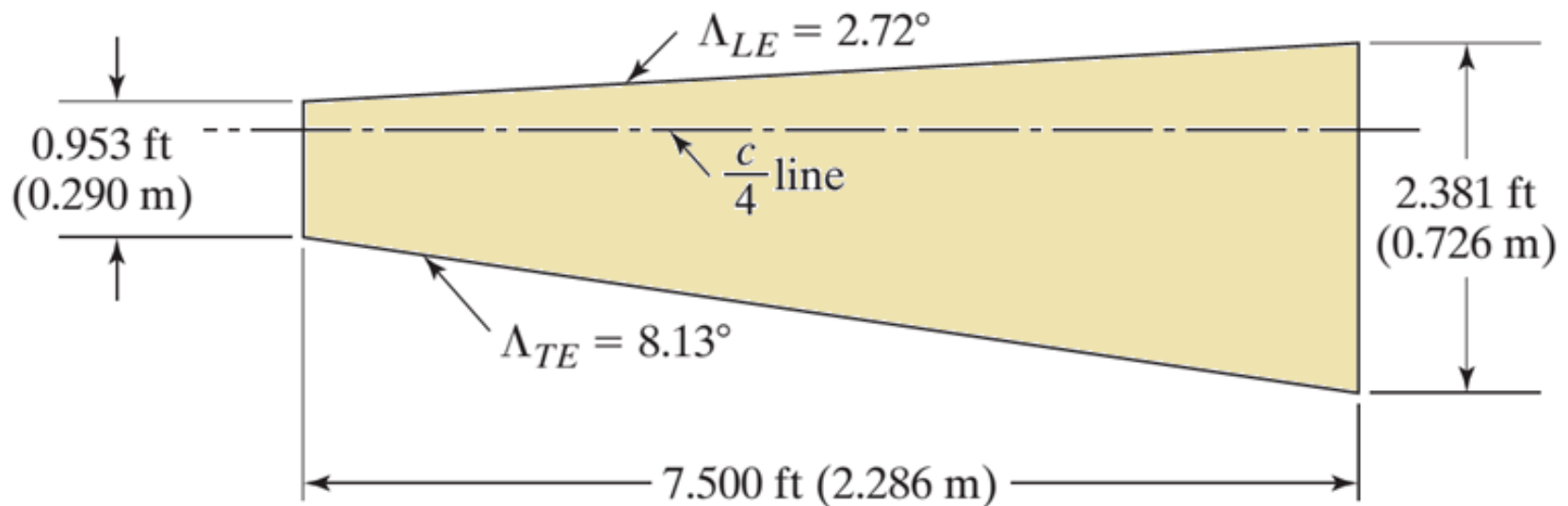


Figure 7.16 Planform for an unswept wing, $AR = 9.00$, $\lambda = 0.40$, airfoil section NACA 65–210.

attack is the same at all spanwise positions. The aspect ratio (AR) of the full wing is 9.00, and the taper ratio λ (c_t/c_r) is 0.40. Since the wing planform is trapezoidal,

Solution

$$S = \frac{1}{2}(c_r + c_t)b = \frac{1}{2}c_r(1 + \lambda)b$$

and

$$AR = \frac{2b}{c_r + c_t}$$

Therefore, the parameter μ in equation (7.26) becomes:

$$\mu = \frac{ca_0}{4b} = \frac{ca_0}{2(AR) \cdot c_r(1 + \lambda)}$$

where c is the local chord, $c(y)$.

Solution

Since the terms are to be evaluated at spanwise stations for $0 \leq \phi \leq \pi/2$ [i.e., $-s \leq y \leq 0$ (which corresponds to the port wing or left side of the wing)],

$$\begin{aligned}\mu &= \frac{a_0}{2(1 + \lambda)AR} [1 + (\lambda - 1) \cos \phi] \\ &= 0.24933(1 - 0.6 \cos \phi)\end{aligned}\tag{7.31}$$

where the equivalent lift-curve slope (i.e., for a two-dimensional flow over the airfoil section a_0) has been assumed to be equal to 2π 1/rad. It might be interesting to know that numerical solutions for lift and vortex-drag coefficients were essentially the same for this geometry whether the series representing the spanwise circulation distribution included 4 terms or 10 terms. Therefore, to help the reader perform the required calculations more easily, a four-term series will be used to represent the spanwise loading. Equation (7.26) becomes:

$$\begin{aligned}\mu(\alpha - \alpha_{0l}) \sin \phi &= A_1 \sin \phi (\mu + \sin \phi) + A_3 \sin 3\phi (3\mu + \sin \phi) \\ &\quad + A_5 \sin 5\phi (5\mu + \sin \phi) + A_7 \sin 7\phi (7\mu + \sin \phi)\end{aligned}\tag{7.32}$$

TABLE 7.1 Values of the Factors for Equation (7.32)

<i>Station</i>	ϕ	$-\frac{y}{s}$ (= $\cos \phi$)	$\sin \phi$	$\sin 3\phi$	$\sin 5\phi$	$\sin 7\phi$	μ
1	22.5°	0.92388	0.38268	0.92388	0.92388	0.38268	0.11112
2	45.0°	0.70711	0.70711	0.70711	-0.70711	-0.70711	0.14355
3	67.5°	0.38268	0.92388	-0.38268	-0.38268	0.92388	0.19208
4	90.0°	0.00000	1.00000	-1.00000	1.00000	-1.00000	0.24933

Since there are four coefficients (i.e., A_1 , A_3 , A_5 , and A_7) to be evaluated, equation (7.32) must be evaluated at four spanwise locations. The resultant values for the factors are summarized in Table 7.1. Notice that since we are considering the left side of the wing, the y coordinate is negative.

For a geometric angle of attack of 4°, equation (7.32) becomes:

$$0.00386 = 0.18897A_1 + 0.66154A_3 + 0.86686A_5 + 0.44411A_7$$

for $\phi = 22.5^\circ$ (i.e., $y = -0.92388s$). For the other stations, the equation becomes:

$$0.00921 = 0.60150A_1 + 0.80451A_3 - 1.00752A_5 - 1.21053A_7$$

$$0.01611 = 1.03101A_1 - 0.57407A_3 - 0.72109A_5 + 2.09577A_7$$

$$0.02263 = 1.24933A_1 - 1.74799A_3 + 2.24665A_5 - 2.74531A_7$$

which is four equations in four unknowns. The solution of this system of linear equations yields:

$$A_1 = 1.6459 \times 10^{-2}$$

$$A_3 = 7.3218 \times 10^{-5}$$

$$A_5 = 8.5787 \times 10^{-4}$$

$$A_7 = -9.6964 \times 10^{-5}$$

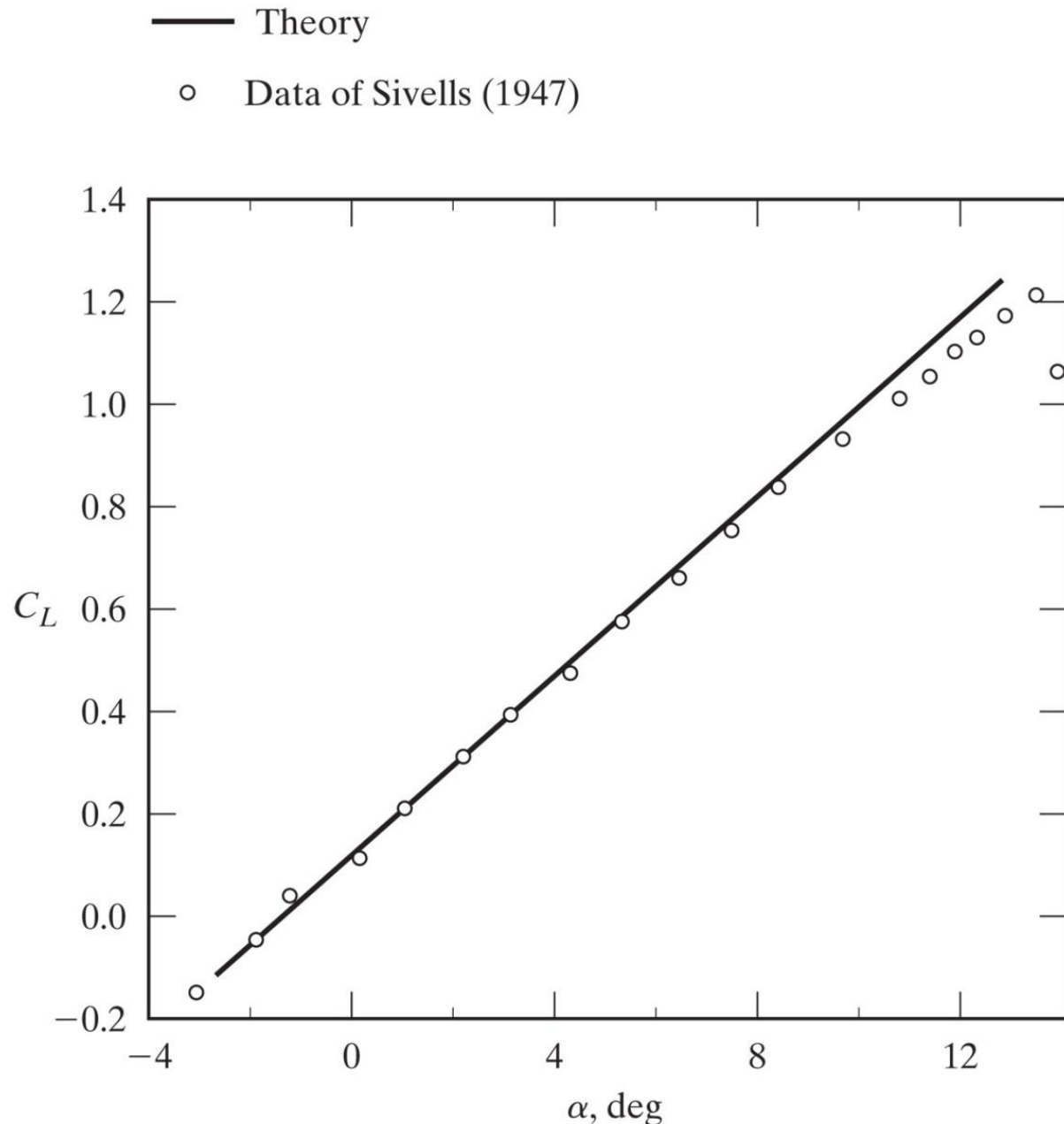
Using equation (7.27), the lift coefficient for an angle of attack of 4° is:

$$C_L = A_1 \pi AR = 0.4654$$

The theoretically determined lift coefficients are compared in Fig. 7.17 with data for this wing. In addition to the geometric characteristics already described, the wing has a dihedral angle of 3° , which we are not modeling. The measurements reported by Sivells (1947) were obtained at a Reynolds number of approximately 4.4×10^6 and a Mach number of approximately 0.17, and our theory assumes inviscid, incompressible flow. In spite of these differences, the agreement between the theoretical values and the experimental values is very good.

The spanwise distribution for the local lift coefficient of this wing is presented in Fig. 7.18. As noted by Sivells (1947), the variation of the section

Figure 7.17
Comparison of the theoretical and the experimental lift coefficients for an unswept wing in a subsonic stream (wing is that of Fig. 7.16).



lift coefficient can be used to determine the spanwise position of initial stall. The local lift coefficient is given by:

$$C_l = \frac{\rho_\infty U_\infty \Gamma}{\frac{1}{2} \rho_\infty U_\infty^2 c}$$

where c is the local chord at a given location along the span, $c(y)$. For the trapezoidal wing under consideration is:

$$C_l(\phi) = 2AR(1 + \lambda) \frac{c_r}{c(\phi)} \sum \{ A_{2n-1} \sin[(2n - 1)\phi] \} \quad (7.33)$$

The theoretical value of the induced drag coefficient for an angle of attack of 4° , as determined using equation (7.29), is:

$$\begin{aligned} C_{Dv} &= \frac{C_L^2}{\pi AR} \left(1 + \frac{3A_3^2}{A_1^2} + \frac{5A_5^2}{A_1^2} + \frac{7A_7^2}{A_1^2} \right) = \frac{C_L^2}{\pi AR} (1 + \delta) \\ &= 0.00766(1.0136) = 0.00776 \end{aligned}$$

and $\delta = 0.0136$. The theoretically determined induced drag coefficients are compared in Fig. 7.19 with the measured drag coefficients for this wing.

Spanwise distribution of the local lift coefficient

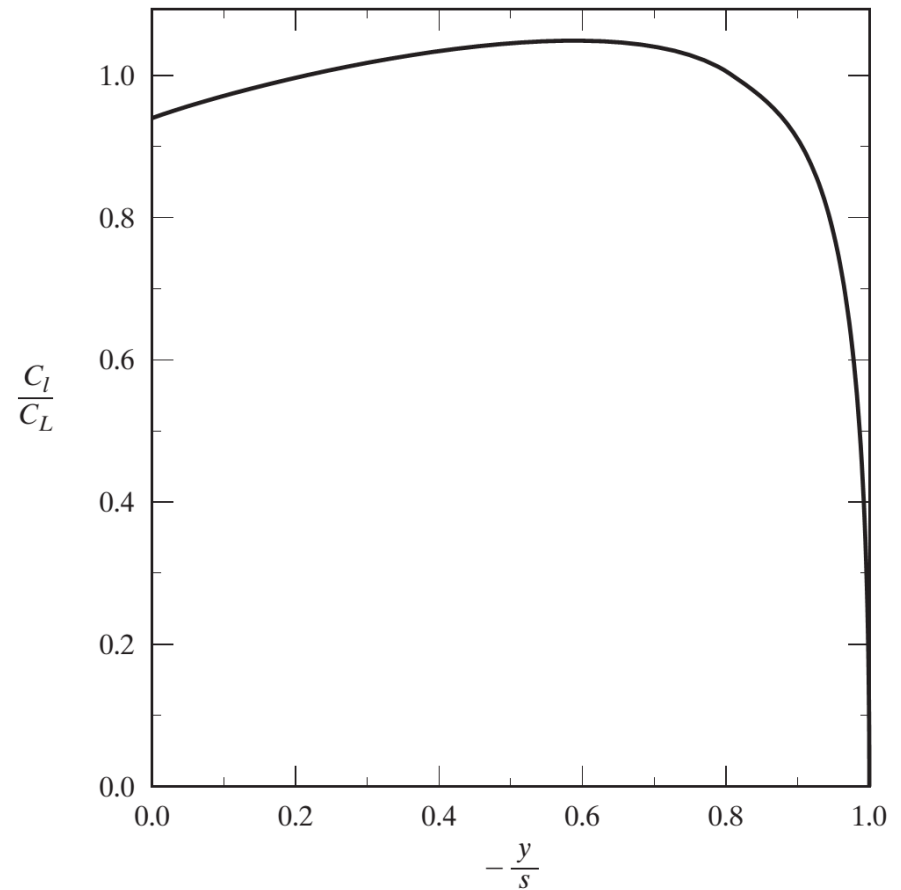
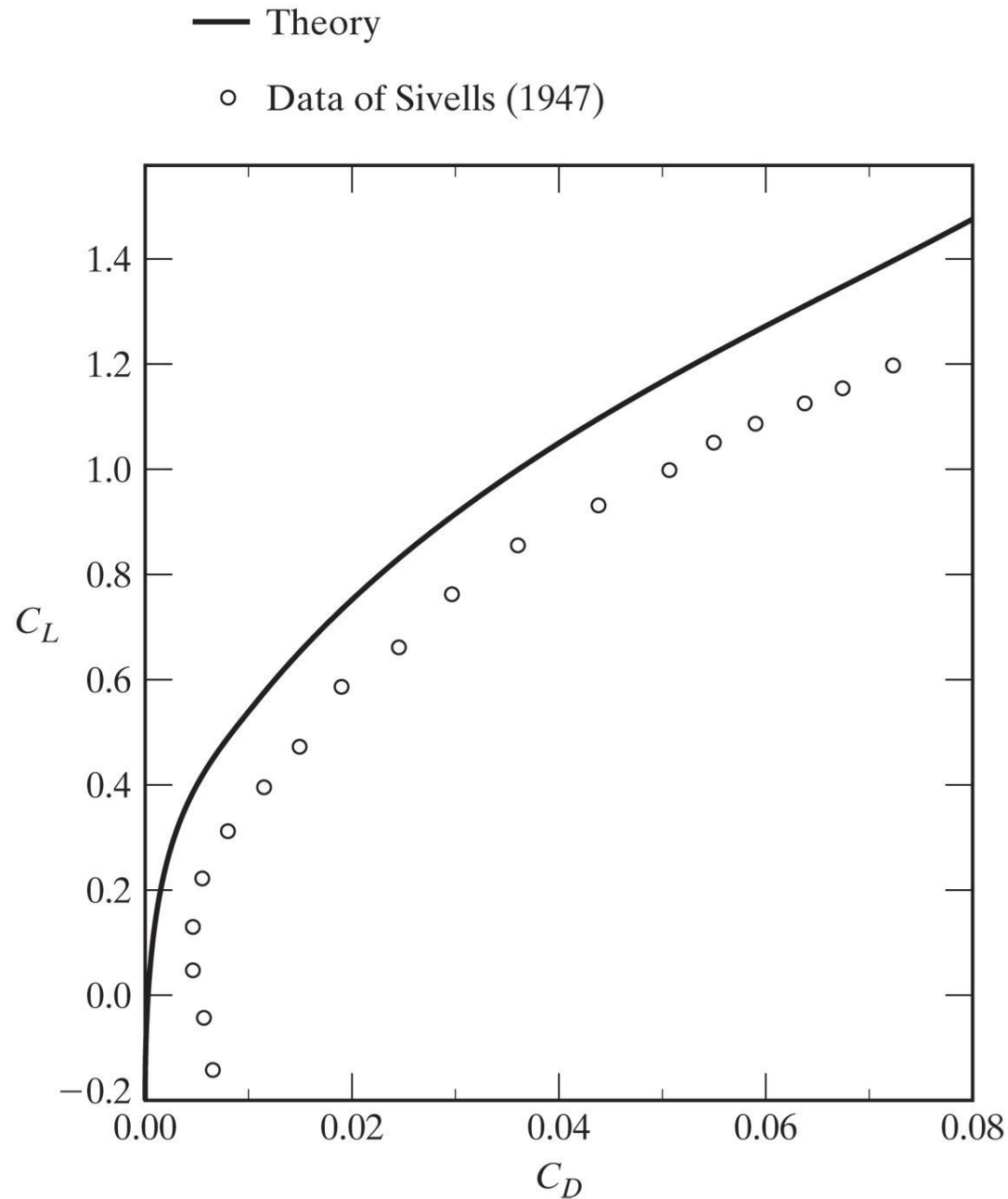


Figure 7.18 Spanwise distribution of the local lift coefficient, $AR = 9$, $\lambda = 0.4$, untwisted wing composed of NACA 65–210 airfoil sections.

As we noted earlier, the theoretical relations developed in this chapter do not include the effects of skin friction. The relatively constant difference between the measured values and the theoretical values is due to the influence of skin friction.

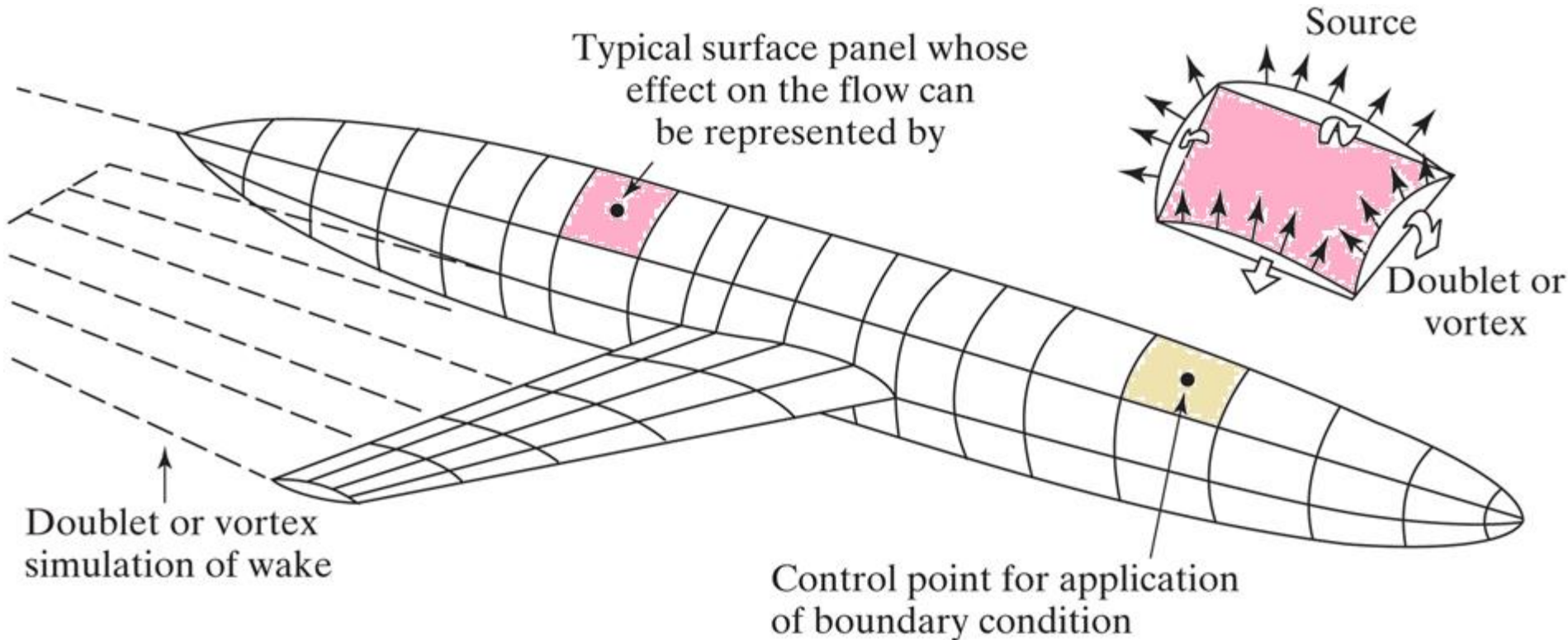
Figure 7.19
Comparison of the theoretical induced drag coefficients and the measured drag coefficients for an unswept wing in a subsonic stream



PANEL METHODS

- Panel methods, have been developed to compute the flow about a thin wing at a small angle of attack so that the resultant flow may be assumed to be steady, inviscid, irrotational, and incompressible.
- The configuration is modeled by a large number of elementary quadrilateral panels.
- For each elementary panel, one or more types of singularity distributions (such as sources, vortices, and doublets) are attached.
- These singularities are determined by specifying some functional variation across the panel whose actual value is set by corresponding strength parameters (source strength, vortex strength, etc.).
- These strength parameters are determined by solving for appropriate boundary condition equations, and once the singularity strengths have been determined, the velocity field and the pressure field can be computed.

Representation of an airplane flow field by panel (or singularity) methods.



Boundary Conditions

- The boundary conditions for the flow field determine the singularity strengths for a panel method.
- Fluid flow **boundary conditions** associated with Laplace's equation are generally of **analysis** or **design** type.
- **Analysis conditions** are employed on portions of the boundary where the geometry is considered fixed, and resultant pressures are desired.
- The permeability of the fixed geometry is known; hence, analysis conditions are of the **Neumann type** (specification of normal velocity).
- **Design boundary conditions** are used wherever a geometry perturbation is allowed for the purpose of achieving a specific pressure distribution.
- Here a perturbation to an existing tangential velocity vector field is made; hence, design conditions are fundamentally of the **Dirichlet type** (specification of potential).

Boundary Conditions

- If the surface of the configuration is impermeable, the normal component of the resultant velocity must be zero at every point of the surface ($\frac{\partial \phi}{\partial n} = 0$).
- Once a solution for ϕ has been found the pressure coefficient at each point on the surface of the boundary can be computed.
- To achieve both a specified pressure distribution and a normal flow distribution on the surface, the position of the surface must, in general, be perturbed, so that the surface will be a stream surface of the flow field.
- The total design problem is thus composed of two problems:
- **The first** is to find a perturbation potential for the surface that yields the desired distribution for the pressure coefficient and
- **the second** is to update the surface geometry so that it is a stream surface of the resultant flow.

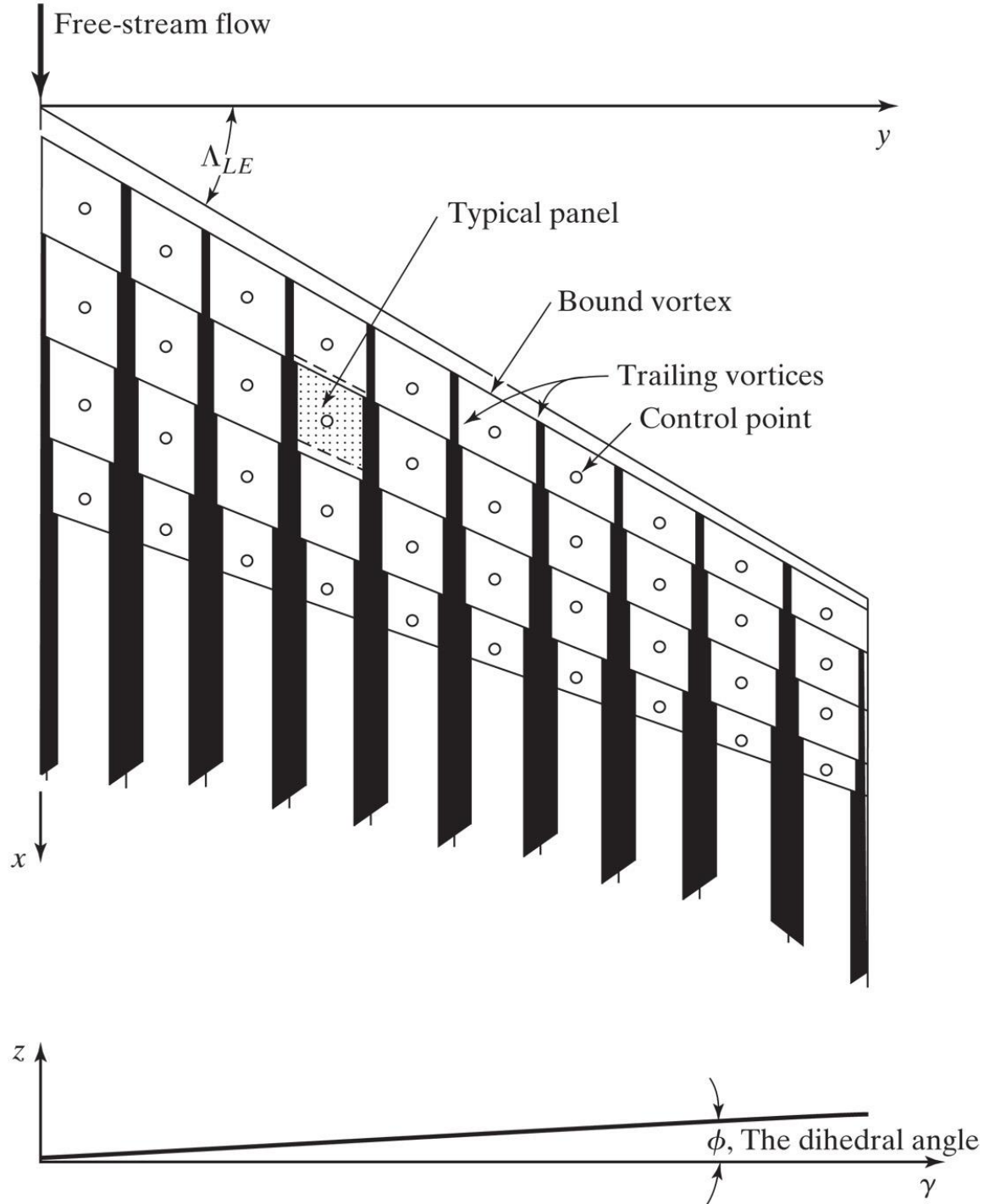
Solution Methods

- The first step in a panel method is to divide the boundary surface into a number of panels.
- A finite set of control points (equal in number to the number of singularity parameters) is selected at which the boundary conditions are imposed.
- The construction of each network requires developments in three areas:
 - (1) the definition of the surface geometry,
 - (2) the definition of the singularity strengths, and
 - (3) the selection of the control points and the specification of the boundary conditions.
- Numerous computer codes using panel-method techniques have been developed since the 1960s, the variations depending mainly on the choice of type and form of singularity distribution, the geometric layout of the elementary panels, and the type of boundary condition imposed.
- The VLM predicts the experimental data very well.

VORTEX LATTICE METHOD

- The VLM represents the wing as a surface on which a grid of horseshoe vortices (from lifting-line theory) is superimposed.
- The velocities induced by each horseshoe vortex at a specified control point are calculated.
- A summation is performed for all control points on the wing to produce a set of linear algebraic equations for the horseshoe vortex strengths that satisfy the boundary condition of no flow through the wing.
- The vortex strengths are related to the wing circulation and the pressure differential between the upper and lower wing surfaces.
- The pressure differentials are integrated to yield the total forces and moments.
- The continuous distribution of bound vorticity over the wing surface is approximated by a finite number of discrete horseshoe vortices.
- The individual horseshoe vortices are placed in trapezoidal panels (also called *finite elements* or *lattices*).

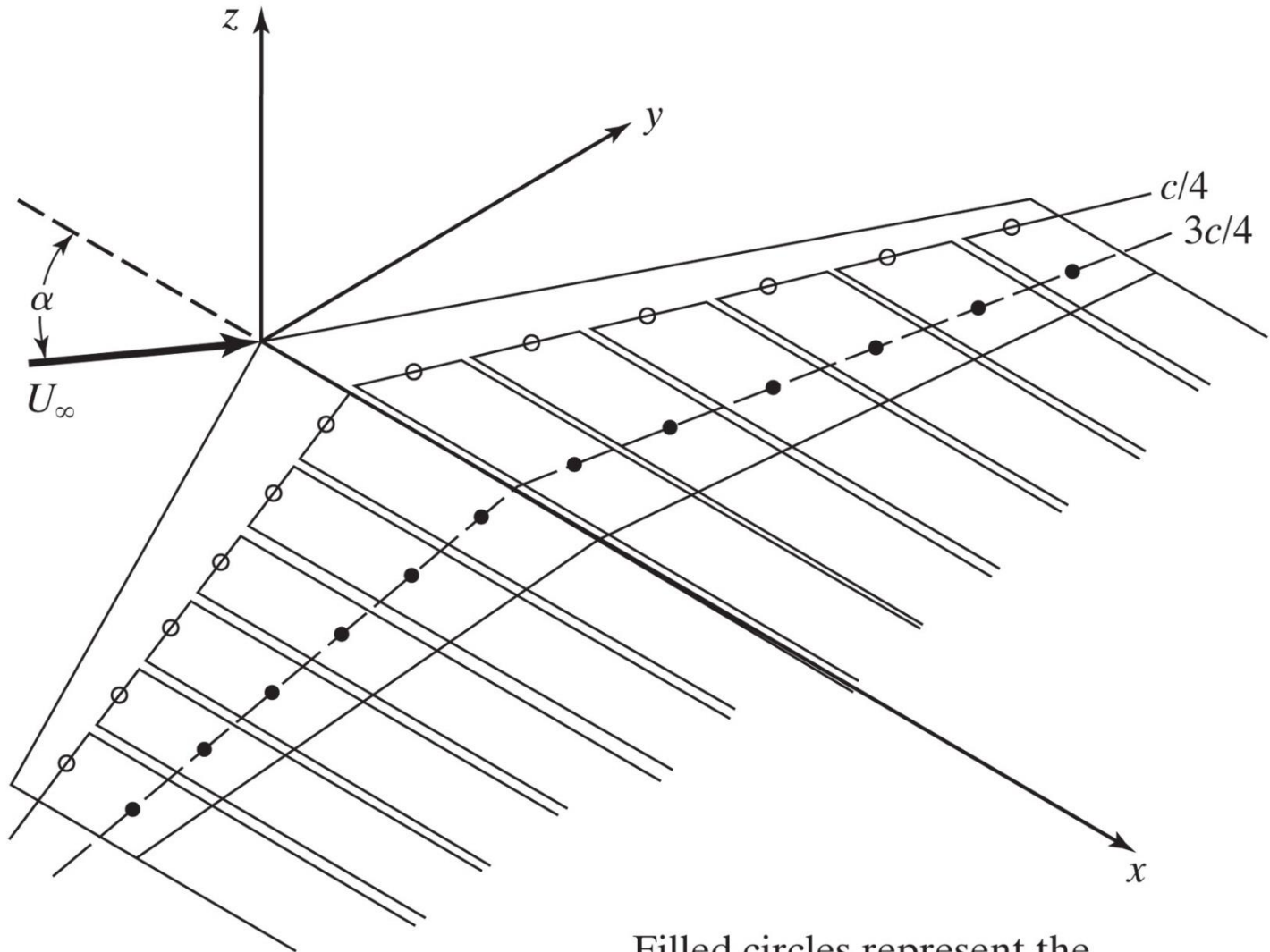
Coordinate system, elemental panels, and horseshoe vortices for a typical wing planform in the vortex lattice method.



VORTEX LATTICE METHOD

- The bound vortex typically coincides with the quarter-chord line of the panel (or element) and is, therefore, aligned with the local sweepback angle.
- The vortex lattice panels are located on the mean camber surface of the wing and, when the trailing vortices leave the wing, they follow a curved path.
- Suitable accuracy can be obtained using linearized theory in which straight-line trailing vortices extend downstream to infinity.
- We assume that the trailing vortices are parallel to the axis of the vehicle.
- This orientation of the trailing vortices is chosen because the computation of the influences of the various vortices (the *influence coefficients*) is simpler.
- Furthermore, these geometric coefficients do not change as the angle of attack is changed.

7.26. Distributed horseshoe vortices representing the lifting flow field over a swept wing.



Filled circles represent the control points

VORTEX LATTICE METHOD

- Application of the boundary condition that the flow is tangent to the wing surface at “the” control point of each of the $2N$ panels (i.e., **there is no flow through the surface**) provides a set of simultaneous equations in terms of the unknown vortex circulation strengths.
- The control point of each panel is centered spanwise on the three-quarter-chord line midway between the trailing-vortex legs.
- Consider the flow over the swept wing in Fig. 7.26 .
- Notice that the bound-vortex filaments for the port (or left-hand) wing are not parallel to the bound vortex filaments for the starboard (or right-hand) wing.
- Thus, for a lifting swept wing, the bound-vortex system on one side of the wing produces downwash on the other side of the wing.
- This downwash reduces the net lift and increases the total induced drag produced by the flow over the finite-span wing.

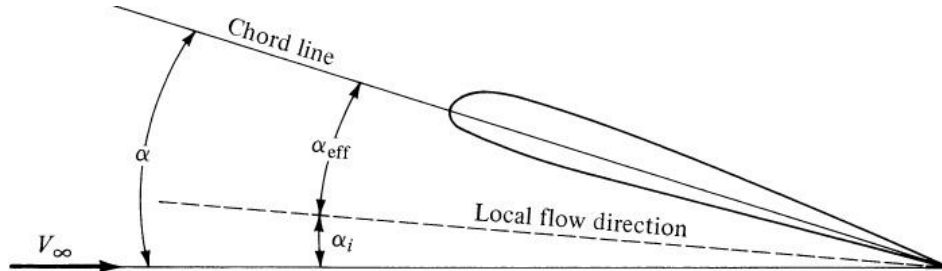
VORTEX LATTICE METHOD

- The downwash resulting from the bound-vortex system is greatest near the center of the wing, while the downwash resulting from the trailing-vortex system is greatest near the wing tips.
- So, for a swept wing the lift is reduced both near the center and near the tips of the wing.

Note: FINITE WING CHANGE IN LIFT SLOPE

Infinite Wing

- In a wind tunnel, the easiest thing to measure is the geometric angle of attack



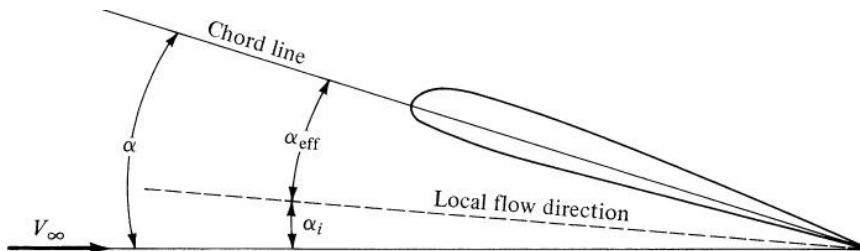
$$\alpha_{geom} = \alpha_{eff} + \epsilon = \alpha_{eff}$$

For infinite wings, there is no induced angle of attack

- The angle you see = the angle the infinite wing 'sees'

Finite Wing

- With finite wings, there is an induced angle of attack
- The angle you see \neq the angle the finite wing 'sees'

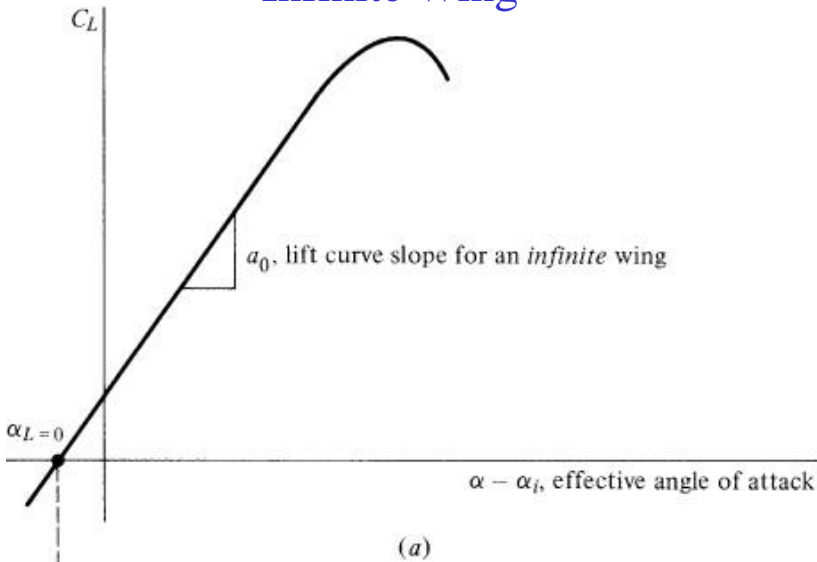


$$\alpha_{geom} = \alpha_{eff} + \epsilon$$

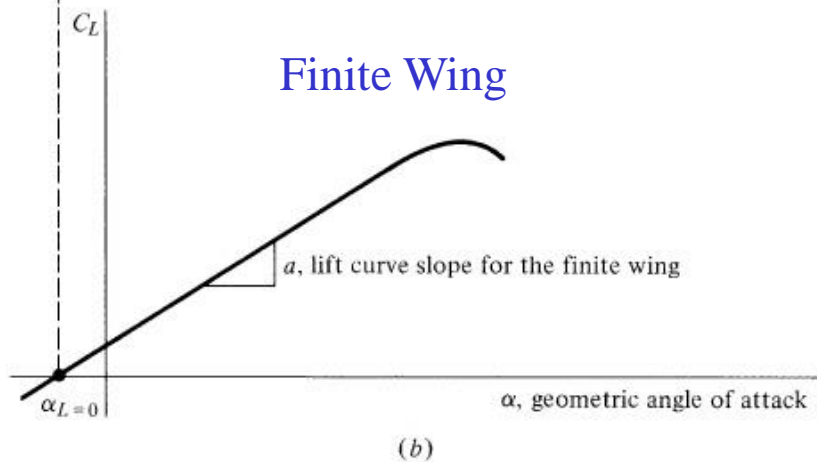
$$\alpha_{geom} = \alpha_{eff} + \epsilon$$

FINITE WING CHANGE IN LIFT SLOPE

Infinite Wing



Finite Wing



- Lift curve for a finite wing has a smaller slope than corresponding curve for an infinite wing with same airfoil cross-section

- Figure (a) shows infinite wing, $\varepsilon = 0$, so plot is C_L vs. α_{geom} or α_{eff} and slope is a_0

- Figure (b) shows finite wing, $\varepsilon \neq 0$
 - Plot C_L vs. what we see, α_{geom} , (or what would be easy to measure in a wind tunnel), not what wing sees, α_{eff}

1. Effect of finite wing is to reduce lift curve slope

- Finite wing lift slope = $a = dC_L/d\alpha$

2. At $C_L = 0$, $\varepsilon = 0$, so $\alpha_{L=0}$ same for infinite or finite wings

- # SUMMARY

Induced drag is price you pay for generation of lift

- $C_{D,i}$ proportional to C_L^2
 - Airplane on take-off or landing, induced drag major component
 - Significant at cruise (15-25% of total drag)
- $C_{D,i}$ inversely proportional to AR
 - Desire high AR to reduce induced drag
 - Compromise between structures and aerodynamics
 - AR important tool as designer (more control than span efficiency, e)
- For an elliptic lift distribution, chord must vary elliptically along span
 - Wing planform is elliptical
 - Elliptical lift distribution gives good approximation for arbitrary finite wing through use of span efficiency factor, e

Minimizing Induced Drag

$$C_{Dv} = \frac{C_L^2}{\pi \cdot AR} (1 + \delta) = \frac{C_L^2}{\pi e \cdot AR}$$

High Aspect Ratio



REALLY HIGH ASPECT RATIO

- L/D ratios can be over 50!
- Aspect ratio can be over 40
- All out attempt to reduce induced drag



Glider



Unmanned

EXAMPLE: NASA HELIOS



- Helios: solar-electric flying wing, designed to operate at extremely high altitudes for long duration, remotely piloted aircraft, **AR = 31:1**
- Helios Prototype designed to fly at altitudes of up to **100,000 feet** on single-day atmospheric science and imaging missions, as well as perform multi-day telecommunications relay missions at altitudes from 50,000 to 65,000 feet.
- Helios Prototype set world altitude record for winged aircraft, 96,863 feet, during a flight in August 2001
- Flight at 100,000 ft. is quite similar to that expected in the Martian atmosphere, so data obtained from the record altitude flight will also help to build NASA's data base for future Mars aircraft designs and missions

Minimizing Induced Drag

Elliptical Plan-form

$$C_{Dv} = \frac{C_L^2}{\pi e \cdot AR}$$

$$e = 1$$



Minimizing Induced Drag



Why Winglets?

- *Equivalent to span extension w/o increased wingspan*
- *Reduces wingtip vortices*
- *Reduces drag*



NASA B-727 Wingtip Vortex Test Flight



Winglets

